Tuning the Solubility, Cellular-Uptake and Activity of Microtubule Stabilizing Ruthenium Polypyridyl Complexes

By

Melissa Reardon

Presented to the Faculty of the Graduate School of

The University of Texas at Arlington in Partial Fulfillment

of the Requirements

for the Degree of

MASTER OF SCIENCE IN CHEMISTRY

THE UNIVERSITY OF TEXAS AT ARLINGTON

AUGUST 2021

ACKNOWLDGEMENTS

First, I would like to thank my advisor, Dr. Frederick M. MacDonnell, for the knowledge and support he has have given me throughout the course of my graduate work. He has patiently helped enhance my knowledge in Chemistry and provided me with the tools to continue to guide myself in research. I am grateful to have been able to work with him and learn valuable lessons both in lab and in life.

I would like to thank my thesis committee members, Dr. Sherri McFarland, Dr. Rasika Dias, and Dr. Purnendu Dasgupta, for their endless support and valuable advice. In addition, I would like to thank Dr. McFarland for helping me become a better scientific writer and encouraging me to submit an NIH F31 grant.

A special thanks to my past and current lab members of Dr. MacDonnell's group: Dr. Nagham Alatrash, Dr. Faiza Issa, Dr. Cynthia Griffith, Radhiyah Himawan, Asiah Himawan, Christian Torres, Matthew Guerrero, and Sarah Abourakbah for your help and support, both personally and professionally, in the lab. Dr. Alatrash, thank you for your endless support, guidance, and effort throughout my time in Dr. MacDonnell's lab. I truly appreciate your friendship and being my graduate school "Mom." Matthew, thank you for all of your help and support as my friend, undergraduate, and now as a master's student.

I would like to thank the Department staff Stephanie Henry, Dr. Brian Edwards, Dr. Roy McDougald, Beth Klimek, Dr. Charles Phillip Shelor, Dr. Delphine Gout, Dr. Bill Cleaver, Jill Howard, Debbie Cooke, and Natalie Croy for their constant assistance and support. Stephanie, I am grateful for your endless guidance, support, and overall assistance during my time in the graduate program, I will always value your friendship. Dr. Brian Edwards and Dr. Roy McDougald for your continuous patience, assistance,

willingness to guide me while I learn new instruments, and the time you spent to help fix instruments, so my research was not delayed immensely. Dr. Shelor and Dr. Dasgupta, for the equipment and technical skills needed to perform my ICP-MS experiments, as well as the additional help from Dr. Shelor for his education so I could run it independently.

I would like to thank my undergraduate mentor Dr. Arsalan Mirjafari for ensuring my understanding of the world of chemistry research and providing the foundation which has assisted my learning. I am so grateful for his endless encouragement and confidence in my success.

My deepest gratitude goes out to my friends Tori Vives, Nicole Cook, Christina Amstutz, Talia Mervosh, Beth Readel, Dr. Michael Wey, Dr. Siqi Du, Andrew Franklin, Brandon Fulton, and more for their endless support. I will be forever grateful. I would also like to thank my family Abuela and Abuelo (Dalia and Onelio Fernandez), Tia Nely Fernandez, Uncle Dan and Aunt Andrea Reardon, Aunt Felicia and Uncle Leo Torres, my brother Eric Reardon, Lexi Riedel and so many more for their understanding and support throughout this time, it is truly appreciated. Also, thank you to my grandparents, Bill and Marie Reardon, for all the love and support in helping me become the person I am today.

Last, but certainly not least I would like to give my deepest thanks to my parents, David and Iraida Reardon, for whom I would like to fully dedicate this Thesis to. They have made me the woman I am today. What they have given me is immeasurable. Thank you for lending your ear, supporting me (afar and in-person), your guidance, love, and so much more. I would not be where I am today without your help and encouragement that I can do anything I put my mind to. Thank you, I love you both so much!

May 29th, 2021

ABSTRACT

Many Ru(II) Polypyridyl Complexes (RPCs) are being investigated as they show potent cytotoxicity and acceptable toleration in animals. Some of these RPCs are thought to target DNA and/or mitochondria in cells. Recently, $[Ru(dip)_3]^{2+}$ (dip= 4,7-diphenylphenanthroline) with cytotoxicity ranging from 1-4 μM, has shown to target microtubules (MTs) and exhibit strong microtubule stabilizing activity (MSA). Determination of $[Ru(dip)_3]^{2+}$:MT stoichiometry was difficult due to poor solubility. Therefore, to study this new metallo-organic target, a less lipophilic RPC is needed to enhance solubility, while still achieving cytotoxicity.

The purpose of this thesis is to test the following hypothesis. We postulate that by systematically altering the dip ancillary ligands of $[Ru(dip)_3]Cl_2$ with more hydrophilic ligand such as 1,10-phenathroline (phen), the biological effects can be maintained and overall display MSA, which is elucidated in Chapter 1.

Chapter 2 outlines the synthetic approach for two less lipophilic complexes, $[Ru(dip)_2phen]Cl_2$ and $[Ru(phen)_2dip]Cl_2$, based on systematically altering dip ancillary ligands with phen, a more hydrophilic ligand. To quantify lipophilicity, the partition coefficients (logP) were determined via the shake-flask method, where lipophilicity was directly related to the number of dip ligands.

Chapter 3 discusses the similarities and differences across these family of complexes. The cytotoxicity against malignant cell lines H358 and MCF-7 was investigated, in which the cytotoxicity correlated with the lipophilicity; $[Ru(phen)_3]Cl_2 << [Ru(phen)_2dip]Cl_2 < [Ru(dip)_2phen]Cl_2 < [Ru(dip)_3]Cl_2$. In both cell lies, cellular uptake displayed a correlation with lipophilicity and sub-cellular localization studies displayed that

as the number of dip ligands decreased, so did their accumulation within the cytoskeleton; $[Ru(dip)_3]Cl_2$ and $[Ru(dip)_2phen]Cl_2$ >40 % in the cytoskeleton. Yet, all RPCs displayed MSA in a tubulin polymerization assay, with $[Ru(dip)_2phen]Cl_2$ and $[Ru(dip)_3]Cl_2$ acting similarly. A MT binding stoichiometry study of $Ru(dip)_2phen]Cl_2$ is discussed, and its findings are compared to isothermal titration calorimetry data obtained previously using $[Ru(dip)_3]Cl_2$.

TABLE OF CONTENTS

ACKNOWLDGEMENTS iv

ABSTRACT vi

LIST OF ILLUSTRATIONS x

LIST OF SCHEMES xii

LIST OF TABLES xiii

LIST OF ABBREVIATIONS xiv

1.1 Cancer Facts and Platinum Based Agents 1
1.2 Ruthenium(II) Polypyridyl Based Agents 3
1.3 Scope of Thesis 9
2.1 Introduction 10
2.2.1 Chemicals 11
2.3 Characterization 12
2.3.1. ^{1}H NMR 12
2.3.2. LC-MS 12
2.3.3. X-ray Crystallography 12
2.3.4 UV-Vis Spectrophotometer 13
2.4 Synthesis 13
2.4.1 Synthesis of $[Ru(phen)_2Cl_2]$ 13
2.4.2 Synthesis of $[Ru(phen)_2dip]Cl_2$ 14
2.4.3 Synthesis of $[Ru(dip)_2Cl_2]$ 15
2.4.4 Synthesis of $[Ru(dip)_2phen]Cl_2$ 15
2.5 Experiments 16
2.5.1 Partition Coefficient Determinations 16
2.6 Results and Discussion 16
2.7 Conclusion 22
3.1 Introduction 23

3.2 Experimental 25
3.2.1 Chemicals 25
3.3 Cell Lines and Cultures 26
3.4 Instrumentation 26
3.4.1 UV-Vis Plate Reader 26
3.4.2 Microwave Digestion Oven 27
3.4.3 ICP-MS 27
3.4.4 UV-Vis Spectrophotometer 28
3.5 Experiments 28
3.5.1 Cytotoxicity 28
3.5.2 Cellular Uptake 29
3.5.3 Bicinchoninic Acid (BCA) 30
3.5.4 Sub-cellular Fractionation 30
3.5.5 Tubulin Polymerization Assay 31
3.5.6 Tubulin Stoichiometry Binding Assay 32
3.6 Results and Discussion 33
3.7 Conclusion 42
APPENDIX 44

A. NMR data 44
B. X-ray crystallography data 46
REFERENCES 51

BIOLOGICAL INFORMATION 63

LIST OF ILLUSTRATIONS

Figure 1.1. Metal-based complexes; (A) FDA approved Platinum based complexes and (B) Ruthenium based complexes that have made it to clinical trials.

Figure 1.2. Referenced Ru(II) polypyridyl complexes; (A) homoleptic complexes and (B) heteroleptic complexes. Partition coefficient of n-octanol and water is defined as $LogP_{o/w}$, which represents a complexes' lipophilicity.

Figure 1.3. MacDonnell lab referenced complexes and the comparison of the structure's lipophilicity to uptake into the cell; (A) dinuclear Ru(II) polypyridyl complexes and (B) mononuclear Ru(II) polypyridyl complexes (where tpphz = tetrapyrido[3,2-a: 2′,3′-c: 3″,2″-h: 2″,3‴-j]phenazine).

Figure 2.1. The family of Ru(II) polypyridyl complexes where the tris-phen complex's ligand is systematically altered with dip ligands until the tris-dip complex is obtained.

Figure 2.2. Labeled ^{1}H NMR of $[Ru(phen)_2dip]Cl_2$ in CD_3CN. Numbers 1-4 and 1'-4' represent the protons on the phen ligands and the letters a-c and ph refer to the protons on the dip ligand. (where ph= phenyl group)

Figure 2.3. Labeled ^{1}H NMR of $[Ru(dip)_2phen]Cl_2$ in CD_3CN. Letters a-c, ph, and a'-c' refer to the protons on the dip ligands and the numbers 1-4 represent the protons on the phen ligand. (where ph= phenyl group)

Figure 2.4. Crystal structure obtained for the $[Ru(phen)_2dip]Cl_2$ complex. Green balls indicate chloride counterions and red balls indicate waters of crystallization. Hydrogen positions are calculated.

Figure 3.1. Among the FDA approved organic-based microtubule targeting agents.

Figure 3.2. Uptake data on both H358 (blue) and MCF-7 (red) cell lines at 37 ˚C of Ru content from the treated family of compounds. The mass of Ru is displayed in ng per million cells that were treated with 20 µM and incubated for 1 h at 37 ˚C which was determined via ICP-MS.

Figure 3.3. Sub-cellular localization data of and MCF-7 cell line at 37 ˚C of Ru content from the treated family of compounds. The Ru (reported as ng per million cells) found in each of the four fractions (nucleus, cytosol, mitochondria/Golgi/ER, cytoskeleton) using QIAGEN compartment kit and Ru ion content analyzed using ICP-MS. In set shows the total Ru mass for each cell and is report as ng per million cells.

Figure 3.4. Sub-cellular localization data of and H358 cell line at 37 ˚C of Ru content from the treated family of compounds. The Ru (reported as ng per million cells) found in each of the four fractions (nucleus, cytosol, mitochondria/Golgi/ER, cytoskeleton) using QIAGEN compartment kit and Ru ion content analyzed using ICP-MS. In set shows the total Ru mass for each cell and is report as ng per million cells.

Figure 3.5. The effect of different ligands on tubulin polymerization is done *in vitro* for the family of compounds. The polymerization causes a change in turbidity and is measured by light transmission at 340 nm. The turbidity increase that indicated tubulin polymerization occurs upon a temperature jump from 4 ˚C to 37 ˚C in the presence of 1 mM GTP and 10 % glycerol in general tubulin buffer (80 mM PIPES pH 6.9, 2 mM $MgCl_2$, and 0.5 mM EGTA). Runs with an additive (complex) were treated with 10 µM solution and each run contained 3 mg/mL tubulin. The light blue plot shows the normal tubulin polymerization growth curve in the absence of any complex. The black plot represents the microtubule stabilization that occurs in the presence of PTX (MSA). The orange, green, red, and dark blue plots represent the effect on tubulin polymerization in the presence of the family of RPCs $[Ru(phen)_3]Cl_2$, $[Ru(phen)_2dip]Cl_2$, $Ru(dip)_2phen]Cl_2$ and $[Ru(dip)_3]Cl_2$, respectively (color and marker indicated in the legend). The plots in this graph are an average of three experiments; error bars (±0.05 OD) are omitted for clarity.

Figure 3.6. The effect of different ligands on tubulin polymerization was done *in vitro* for the family of compounds in the presence of BSA. The polymerization causes a change in turbidity and is measured by light transmission at 340 nm. The turbidity increase that indicated tubulin polymerization occurs upon a temperature jump from 4 ˚C to 37 ˚C in the presence of 1 mM GTP and 10 % glycerol in general tubulin buffer (80 mM PIPES pH 6.9, 2 mM $MgCl_2$, and 0.5 mM EGTA). Runs with an additive (complex) were treated with 10 µM solution, 80 µM BSA solution and each run contained 3 mg/mL tubulin. The light blue plot shows the normal tubulin polymerization growth curve only in the presence of BSA. The black plot represents the microtubule stabilization that occurs in the presence of PTX (MSA) with BSA present. The orange, green, red, and dark blue plots represent the effect on tubulin polymerization in the presence of the BSA and the family of RPCs $[Ru(phen)_3]Cl_2$, $[Ru(phen)_2dip]Cl_2$, $Ru(dip)_2phen]Cl_2$ and $[Ru(dip)_3]Cl_2$, respectively (color and marker indicated in the legend). The plots in this graph are an average of three experiments; error bars (±0.05 OD) are omitted for clarity.

Figure A.1. 1H NMR of $[Ru(phen)_3]Cl_2$ in DMSO.

Figure A.2. 1H NMR of $[Ru(phen)_2dip]Cl_2$ in CD_3CN.

Figure A.3. COSY 1H NMR of $[Ru(phen)_2dip]Cl_2$ in CD_3CN.

Figure A.4. 1H NMR of $[Ru(dip)_3]Cl_2$ in DMSO.

Figure A.5. 1H NMR of $[Ru(dip)_2phen]Cl_2$ in CD_3CN.

Figure A.6. COSY 1H NMR of $[Ru(dip)_2phen]Cl_2$ in CD_3CN.

LIST OF SCHEMES

Scheme 2.1. The synthesis route for the preparation of $[Ru(phen)_2dip]Cl_2$. The synthesis route of $[Ru(dip)_2phen]Cl_2$ is also implied based on the starting material (top reaction) using dip instead of the phen ligand and the bottom reaction starting with $[Ru(dip)_2Cl_2]$ and using phen instead of the dip ligand. The mmol amount of each reagent and percent yield are indicated.

LIST OF TABLES

Table 1.1. MacDonnell lab referenced complexes and data comparing Ru(II) polypyridyl complexes lipophilicity and cytotoxicity.

Table 2.1. Crystal data and structure refinement.

Table 2.2. LogP values in octanol/buffer (o/b) and octanol/water (o/w) of the studied compounds.

Table 3.1. Outlined data obtained from the cytotoxicity (H358 and MCF-7) of the studied compounds. The LogP values in octanol/buffer (o/b) and octanol/water (o/w) are also outlined for comparison.

Table 3.2. ITC thermodynamic binding data for $[Ru(dip)_3]^{2+}$, DTX, and colchicine with both tubulin and preformed microtubules done previously in the MacDonnell lab (reported as association constants, Tubulin + Complex ⇌ Tubulin-Complex).

Table 3.3. Data obtained to determine the stoichiometry of $Ru(dip)_2phen]Cl_2$ (indicated as "Ru") to tubulin in the presence of albumin (BSA). Protein concentration in the pellet was determined by BSA and reported as nmol. Ru concentration in the pellet was determined using UV-Vis spectrophotometry and Beer's Law, which is reported as nmol. "Ru/BSA" was subtracted from "Tubulin/BSA/Ru", and the remainder was reported as "corrected BSA/Ru".

Table A.1. Atomic coordinates and equivalent displacement parameters U_{eq} ($Å^2$) for the $C_{48}H_{40}Cl_2N_6O_4Ru_1$ crystal structure.

Table A.2. Anisotropic Atomic Displacement Parameters ($Å^2$) for the $C_{48}H_{40}Cl_2N_6O_4Ru_1$ crystal structure.

Table A.3. Main Atomic Distance (Å) for the $C_{48}H_{40}Cl_2N_6O_4Ru_1$ crystal structure.

Table A.4. Main Bonds Angles (˚) for the $C_{48}H_{40}Cl_2N_6O_4Ru_1$ crystal structure.

LIST OF ABBREVIATIONS

A2780	Ovarian cancer cell line
bpy	2,2’-bipyridine
BCA	Bicinchoninic acid
BSA	Bovine serum albumin
CD_3CN	Deuterated acetonitrile
$(CD_3)_2CO$	Deuterated acetone
$(CD_3)_2SO$	Deuterated dimethyl sulfoxide
Cisplatin	*cis*-Diamminedichloroplatinum(II)
Cl^-	Chloride
d	Doublet
dd	Doublet of doublets
dip	4,7-diphenyl-1,10-phenanthroline
DMF	Dimethylformamide
DMSO	Dimethyl sulfoxide
DNA	Deoxyribonucleic acid
dppz	Dipyrido[3,2-a:2’,3’-c]phenazine
DTX	Docetaxel
ε	Extinction coefficient
EGTA	(ethylene glycol-bis(β-aminoethyl ether)-N,N,N′,N′-tetraacetic acid)
EI-MS	Electron Impact Ionization Mass Spectrometry
ER	Endoplasmic Reticulum
FBS	Fetal bovine serum
FDA	Food and Drug Administration

GTB	General tubulin buffer
GTP	Guanosine-5'-triphosphate
^{1}H	Proton
H358	Human non-small cell lung carcinoma
IC_{50}	Half maximal inhibitory concentration
ICP-MS	Inductively coupled plasma mass spectrometry
IP	Intraperitoneal
IT-139	trans-[tetrachloridobis(1H-indazole)ruthenate(iii)]
ITC	Isothermal titration calorimetry
KP1019	indazolium trans-[tetrachlorobis(1H-indazole)ruthenate(III)]
L-L	Bidentate ligand
LC-MS	Liquid chromatography-mass spectroscopy
LiCl	Lithium Chloride
LogP	Partition coefficient
m	Multiplet
M	Ru(II) polypyridyl complex in LC-MS analysis
MCF-7	Non-small cell lung carcinoma
MDA	Microtubule destabilizing agent
me_4phen	3,4,7,8-tetramethylphen-1,10-phenanthroline
$MgCl_2$	Magnesium chloride
MSA	Microtubule stabilizing agent
MT	Microtubule
MTA	Microtubule targeting agent
MTT	3-(4,5-Dimethylthiazol-2-yl)-2,5-diphenyltetrazolium bromide

N-N	Bidentate ligand
NAMI-A	[ImH][trans-$RuCl_4$(DMSO)(Im)]
NCI	National Cancer Institute
NMR	Nuclear Magnetic Resonance
o/w	Octanol/water
o/b	Octanol/buffer (PBS)
P^{4+}	$[(phen)_2Ru(tatpp)Ru(phen)_2]^{4+}$
PBS	Phosphate buffered saline
PF_6^-	Hexafluorophosphate
Ph	Phenyl group
Phen	1,10-phenanthroline
PIPES	1,4-Piperazinediethanesulfonic acid, Piperazine-1,4-bis(2-ethanesulfonic acid), Piperazine-N,N′-bis(2-ethanesulfonic acid)
P_{Ph}^{4+}	$[(dip)_2Ru(tatpp)Ru(dip)_2]^{4+}$
Pt	Platinum
PTX	Paclitaxel
RIPA	Radioimmunoprecipitation assay buffer
RPC	Ruthenium(II) polypyridyl complex
Ru	Ruthenium
Ru red	$[(NH_3)_5Ru\text{-}O\text{-}Ru(NH_3)_4\text{-}O\text{-}Ru(NH_3)_5]^{6+}$
s	Singlet
t	Triplet
Tatpp	9,11,20,22-tetraazatetrapyrido[3,2-a:2’,3’-c:3’‘,2’‘-l:2’“,3’“-n]pentacene
TMS	Tetramethylsilane

TPB	Tubulin polymerization buffer
tpphz	Tetrapyrido[3,2-a: 2′,3′-c: 3″,2″-h: 2″,3‴-j]phenazine
UV	Ultraviolet
VIS	Visible

CHAPTER 1

Cytotoxic Ru(II) Polypyridyl Complexes and the Development of Ruthenium Complexes that Target Microtubules

1.1 Cancer Facts and Platinum Based Agents

Cancer is a global health crisis. In 2019, the US alone had an estimated 1,762,450 new cancer diagnoses and 606,880 deaths.[1] One of the most widely used anti-cancer agents is cisplatin (shown in Figure 1.1A), a DNA-damaging metallodrug based on platinum (Pt) which is administered systemically, and often results in debilitating short- and long-term side-effects and acquired resistance.[2–7]

Cisplatin resistance is problematic given that it is the main treatment plan for many cancers. Patients with ovarian cancer who are treated with cisplatin show an initial response of nearly 80%, but within two years, about 75% of these patients become resistant.[5] A similar trend exists for other varieties of cancer treated with cisplatin (e.g., breast, small cell lung, prostate, colorectal, and esophageal cancer).[8–15] The resistance to cisplatin, in addition to its severe side effects, led to FDA-approval of carboplatin and oxaliplatin (Figure 1.1A). Carboplatin is the only other Pt-based drug to gain widespread approval for treating a range of cancers; oxaliplatin is only approved for colorectal cancer (and is the only Pt-based compound that is active against colorectal cancer). These Pt-based drugs operate by a similar mechanism to cisplatin which involves dissociation of one or more chloro (Cl^-) ligands followed by covalent modification of biomolecules, such as DNA. This mechanism has been implicated in off-target protein binding, causing side-effects with severity linked to the lability of these Cl^- ligands. Even when these Pt-based drugs are used in combination therapy, both resistance and dose-limiting side-effects

often prevent curative outcomes. Due to the overall success of cisplatin and its derivatives as chemotherapeutic agents, the use of transition-metal complexes and their ability to interact within the cell (in particular with DNA) has sparked an interest in the exploration of transition-metals as potential chemotherapeutic agents.[8,16] However, despite the success of several Pt-based cancer drugs and the use of radioactive metals in cancer therapy and diagnostics, metallo-pharmaceuticals as anticancer agents remain underdeveloped. Although Pt-based agents are still a focus, alternative metallo drugs are being sought with prospective ability to treat a broader spectrum of tumors and/or offer decreased cytotoxicity.

Ruthenium (Ru)-based agents with labile Cl^- ligands demonstrate promising potential with similar ligand exchange kinetics to Pt, but as a d^6 metal. Cytotoxic Ru-based agents that have made it to human clinical trials were labile, similar to cisplatin, which also affected their biological activity with off-target protein binding. Some of the octahedral Ru-based complexes that have shown a significant cytotoxicity toward cancer cells both *in vitro* and *in vivo* are IT-139 (trans-[tetrachloridobis(1H-indazole)ruthenate(iii)]), KP1019 (indazolium *trans*-[tetrachlorobis(1H-indazole)ruthenate(III)]), and NAMI-A (ImH[*trans*-ImDMSORuCl_4]). However, these type of labile Ru-complexes were not competitive with cisplatin (Figure 1.1B).[4,17]

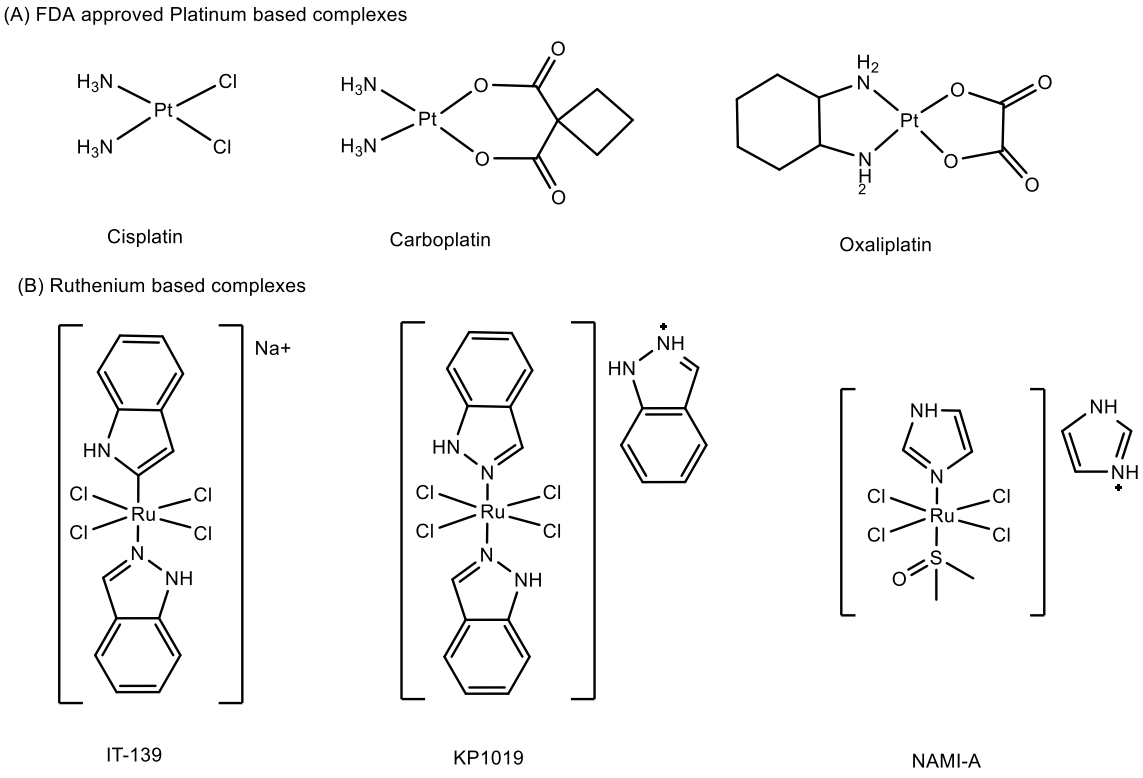

Figure 1.1. Metal-based complexes; (A) FDA approved Platinum based complexes and (B) Ruthenium based complexes that have made it to clinical trials.[4,7,8,16,17]

1.2 Ruthenium(II) Polypyridyl Based Agents

The properties in which scientists have found Ru to be an ideal metal for biological applications are: (i) ligand exchange kinetics (similar to Pt), (ii) range of accessible oxidation states, and (iii) ability to mimics iron's binding within the body.[4,18–20] Transition metal polypyridyl complexes have more inert N-donor polypyridine ligands (coordinatively saturated and substitutionally inert), which allows them to remain intact in biological systems. These Ru-based complexes are called Ru(II) polypyridyl complexes (RPCs). Additionally, their high affinity for DNA (similar to cisplatin's affinity) makes this type of metallo-drug an interesting prospect.[19] Investigation of some RPCs have shown to target other cellular compartments, such as mitochondria and Endoplasmic Reticulum (ER).[21] Furthermore, many promising drugs that undergo human clinical trials are rejected due

to their low solubility and/or increasing amount of excipients needed in order to reach a cytotoxic concentration. A common characteristic of these drugs is their electroneutrality. This has led to the development of charged complexes that utilize Cl^- anions to aid in solubility.[13,15,17,18,20,22]

Some RPCs are considered inert bidentate complexes. Dwyer and coworkers discovered and investigated an RPC known as $[Ru(phen)_3]Cl_2$ (where phen= 1,10-phenanthroline), shown in Figure 2.1A. This complex was found to be inert in a variety of ways: stability in concentrated acids and bases, when the complex was administered intraperitoneally (IP) into mice it was unmetabolized in urine, and when the complex was administered orally to sheep it remained intact within the feces. Unfortunately, this complex was not very cytotoxic against cancer with IC_{50} (half maximum inhibitory concentration, *in vitro*) values well over 50 μM across a majority of cell lines (cytotoxicity is low IC_{50} values, ≥10 μM).[22–25] Due to their inertness and ligand kinetic similarities to Pt-based drugs, scientists have continued to investigate a variety of RPCs for cytotoxic behavior.

In addition to cytotoxicity, quantifying the uptake of a complex is important. Uptake of a complex into a cell requires cell membrane penetration, which is controlled by multiple factors. Pukett and Barton demonstrated that the level of uptake is affected by changing one of the ligands on the homoleptic complexes $[Ru(me_4phen))_3]Cl_2$, $[Ru(phen)_3]Cl_2$, or $[Ru(dip)_3]Cl_2$ to dppz ($[Ru(N\text{-}N)_2dppz]^{2+}$; N-N: me_4phen, phen, dip), shown in Figure 1.2A and 1.2B (where dip = 4,7-diphenylphenanthroline and dppz = dipyrido[3,2-a:2',3'-c]phenazine). It was postulated this may be due to lipophilic effects.[26] Fujita et al. determined a complex's degree of lipophilicity is based on the octanol/water partition

coefficient ($LogP_{o/w}$).[27] This logP value provides an idea of how soluble the complex is, as well as a factor to consider when analyzing its uptake and localization within the cell. Glazer and coworkers compared ligand modification and biological activity of Ru-based complexes. They found the complex $[Ru(dip)_3]^{2+}$ was more lipophilic, entered the cells at a higher quantity, and was more cytotoxic, than the hydrophilic complex, [Ru(bathophenanthroline disulfonate)$_3$]^4.[28] Overall, scientists have seen a trend that the more lipophilic complexes seem to enter the cell more that hydrophilic complexes.

The MacDonnell lab compared dinuclear Ru complexes, $[(phen)_2Ru(tatpp)Ru(phen)_2]^{4+}$ and $[(phen)_2Ru(tatpp)Ru(phen)_2]^{4+}$ (where tatpp= 9,11,20,22-tetraazatetrapyrido[3,2-a:2′,3′-c:3″,2″-l:2‴,3‴-n]pentacene), shown in Figure 1.3A. Changing the ancillary ligands from phen to dip altered lipophilicty, with $LogP_{o/b}$ (octanol/buffer, phosphate buffered saline or PBS pH 7.4) values from -0.6 to 1.7. These $LogP_{o/b}$ values correlated to theobserved difference in uptake; $[(phen)_2Ru(tatpp)Ru(phen)_2]^{4+}$ < $[(phen)_2Ru(tatpp)Ru(phen)_2]^{4+}$. In addition, the MacDonnell lab also investigated the impact lipophilicity has on cytotoxicity with a variety of mononuclear RPCs. They synthesized the complexes in Figure 1.2A and 1.3B as chloride salts and investigated their cytotoxicity toward the MCF-7 (human breast cancer) cell line and lipophilicity as partition coefficients ($LogP_{o/b}$). The observed trend between the complexes was that cytotoxicity increased with lipophilicity which was controlled by altering the ancillary ligands (data in Table 1.1).[24] Pukett and Barton, amongst others, observed that lipophilicity impacts cellular uptake; this trend was prominent in the Ru-based complexes studied by the MacDonnell lab.[26,28–30]

Many of these RPCs and the known Ru(III) complexes, *e.g.* NAMI-A and IT-139 as shown in Figure 1, are thought to localize mainly in the nucleus and/or mitochondria.[21] Recently, a subset of these RPCs has shown to target microtubules (MTs) and disrupt

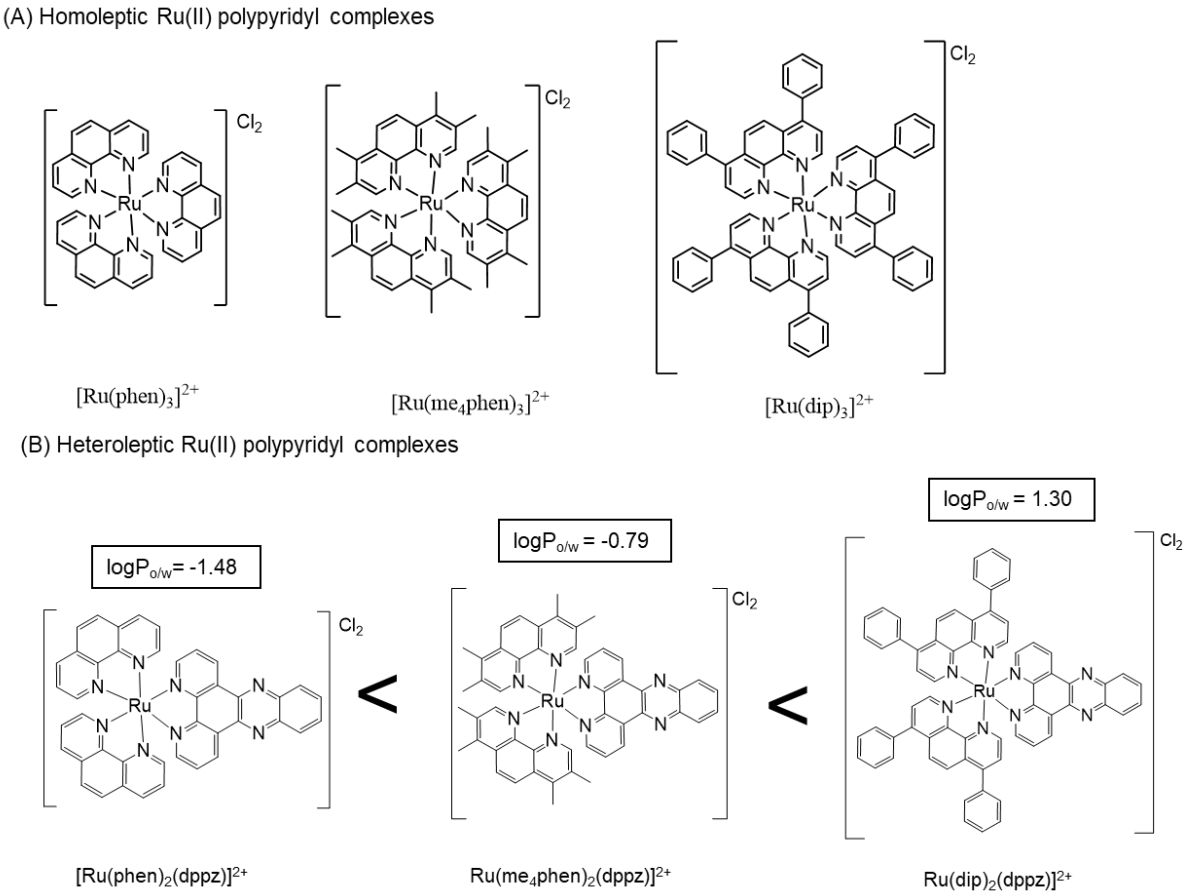

Figure 1.2. Referenced Ru(II) polypyridyl complexes; (A) homoleptic complexes and (B) heteroleptic complexes. Partition coefficient of n-octanol and water is defined as $logP_{o/w}$, which represents a complexes' lipophilicity.[24,25,51,78]

normal MT dynamics by stabilizing them. The RPC $[Ru(dip)_3]^{2+}$ is one such complex with IC_{50} ranging from 1-4 μM and strong microtubule stabilizing activity (MSA) seen in live cells.[31] Microtubules (MTs) are highly dynamic polymers of tubulin that form an integral part of the cytoskeleton. They are crucial in maintaining the structure of the cell and are involved in processes critical to cell survival (e.g., intracellular transport and cell division).

As such, MTs represent an attractive target for anticancer therapy. Drugs that target MTs are known as microtubule targeting agents (MTAs) and include several important anti-cancer drugs such as taxanes and vina alkaloids (which are FDA approved heterocyclic

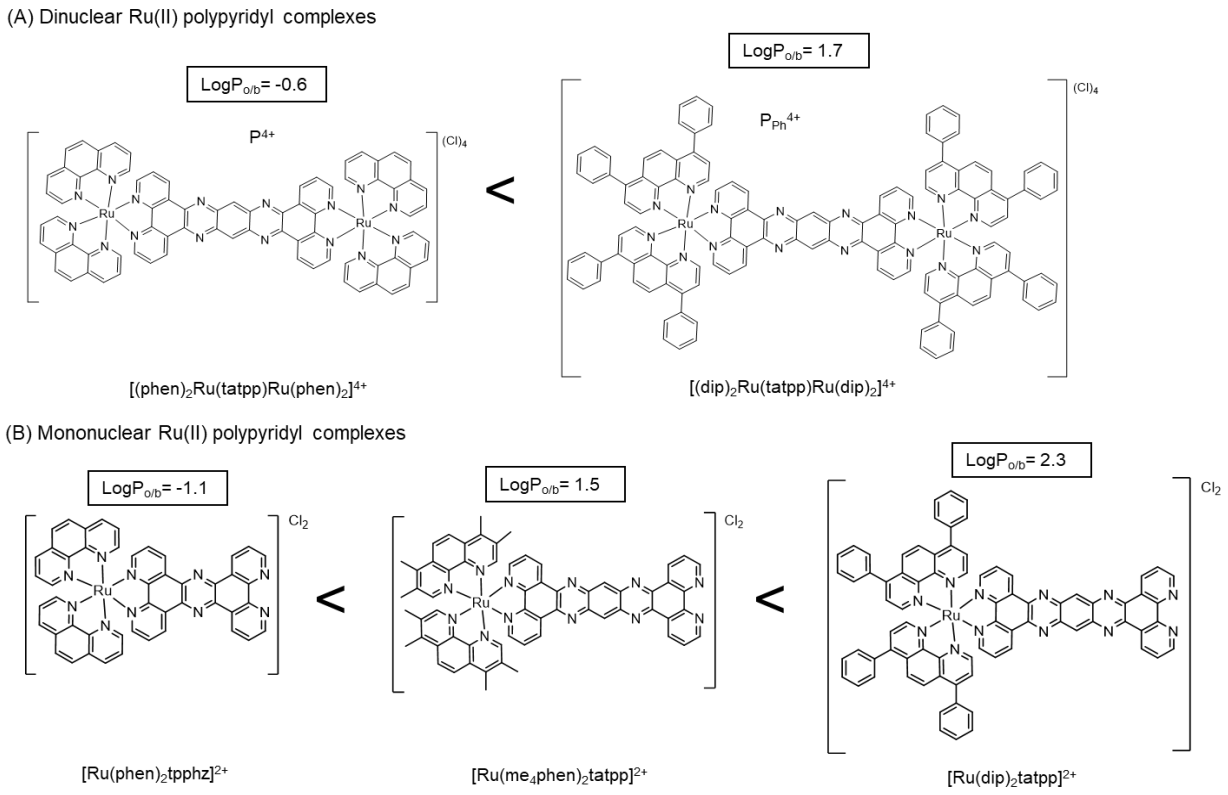

Figure 1.3. MacDonnell lab referenced complexes and the comparison of the structures lipophilicity to uptake into the cell; (A) dinuclear Ru(II) polypyridyl complexes and (B) mononuclear Ru(II) polypyridyl complexes (where tpphz = tetrapyrido[3,2-a: 2′,3′-c: 3″,2″-h: 2″,3‴-j]phenazine).[24,28]

organic molecules typically isolated from natural sources like plants). MTAs are among the most effective agents for solid tumor treatments, since disrupting MT dynamics is generally fatal to the cell.

$[Ru(dip)_3]^{2+}$ was the first organo-metallic complex found to target MTs and exhibit MSA with low micromolar cytotoxicity in malignant cell lines. Unlike organic natural product-based MTAs with synthetic routes can exceed 40 steps, RPCs have relatively

simple structures and are generally easy to prepare in quantity.[31–40] Simple ions such as As^{3+}, Pb^{2+}, and Hg^{2+}, are the only reports to our knowledge of metal complexes targeting MT in cells.[41–43] To our knowledge, there are only two other reports on Ru interaction with tubulin; these studies investigated Ru in respect to the assembly/disassembly and binding of MT *in vitro*. In general, Mg^{2+} seems to promote assembly, whereas Ca^{2+} inhibits assembly, but the mechanism for inhibition is not fully understood.[44–46] This group used "Ru red," an ammoniated Ru oxychloride polymer like structure ($[(NH_3)_5Ru\text{-}O\text{-}Ru(NH_3)_4\text{-}O\text{-}Ru(NH_3)_5]^{6+}$) with various polymer lengths, as a probe for Ca^{2+} to investigate this function, since Ru red had been used previously as a probe for Ca^{2+} binding sites. Their findings suggest that Ru red is a microtubule destabilizing agent (MDA), which reacts differently than our robust and fully characterized complex, $[Ru(dip)_3]^{2+}$.[31,47,48] Another organometallic reported to compound interact with MT, that contains no Ru, is $Os_3(CO)_{10}(NCMe)_2$. This trinuclear osmium carbonyl cluster induces stabilization of MT by the loss of the MeCN group, followed by the osmium interaction with the tubulins' sulfhydryl functional groups.[49]

Table 1.1. MacDonnell lab referenced complexes and data comparing Ru(II) polypyridyl complexes lipophilicity and cytotoxicity.

Complex	$LogP_{o/b}$	$MCF\text{-}7_{IC50}$
$[Ru(phen)_3]^{2+}$	-1.1[a]	>50 μM[b]
$[Ru(phen)_2dppz]^{2+}$	-0.2[a]	>50 μM[c]
$[Ru(phen)_2tpphz]^{2+}$	-0.2[a]	26 μM ± 3.0[d]
$[Ru(me_4phen)_3]^{2+}$	1.6[a]	23 μM ± 3.0[b]
$[Ru(me_4phen)_2tatpp]^{2+}$	1.5[a]	18 μM ± 2.0[b]
$[Ru(dip)_3]^{2+}$	1.9[a]	1.5 μM ± 0.2[b]
$[Ru(dip)_2tatpp]^{2+}$	2.3[a]	1.4 μM ± 0.2[b]
Cisplatin	$-2.3^{a}_{o/w}$	12 μM ± 1.2[d]

[a](Alatrash, MS Thesis, December 2012)[50],[b](Alatrash, ChemMedChem 2017)[24],[c](Puckett, JACS 2007)[51],[d](Gill, ChemBioChem 2011)[30]

1.3 Scope of Thesis

We postulate that by systematically replacing the dip ancillary ligand of $[Ru(dip)_3]Cl_2$ with more hydrophilic ligands, such as 1,10-phenathroline (phen), the biological effects can be maintained and ultimately maintain MT effects.

CHAPTER 2

Tuning the Lipophilicity of Microtubule Targeting Ru(II) Polypyridyl Complexes

2.1 Introduction

The ability of the Ru(II) polypyridyl complex (RPC), tris(4,7-diphenyl-1,10-phenanthroline)ruthenium(II) chloride ($[Ru(dip)_3]Cl_2$), to specifically target and stabilize microtubules in cultured malignant human cells suggest that related RPCs may be similarly active and perhaps show even better uptake, enhanced potency, and be better tolerated *in vivo*. $[Ru(dip)_3]Cl_2$ is a potent cytotoxin, with IC_{50}'s ranging from 1-4 µM across a majority of cell lines. Unfortunately, it is also quite neurotoxic, presumably due to its ability to inhibit acetylcholine esterase, with a maximum tolerated dose of 6 mg complex per kg mouse body weight. By comparison, the DNA cleaving and cytotoxic RPC, $[(phen)Ru(tatpp)Ru(Phen)_2]Cl_4$, has a MTD of 100 mg/kg, indicating a wide range of MTDs are seen within RPCs.

$[Ru(dip)_3]Cl_2$ is exceptionally lipophilic with a $logP_{o/w}$ of 1.9, yet can be dissolved in water, providing it is first dissolved in a little DMSO and then diluted with water or buffer (final DMSO <1% on a volume basis). Despite all efforts, we are unable to directly dissolve $[Ru(dip)_3]Cl_2$ in water and this solubility issue has led us to question if the dissolved complex is not aggregated in some form. Attempts to measure the binding stoichiometry of $[Ru(dip)_3]^{2+}$ with tubulin (either in its polymerized state or as free heterodimers) always gave unreasonably high ratios, i.e. 5:1 Ru:tubulin. We note that the isothermal titration calorimetry showed a clean equivalence point at one $[Ru(dip)_3]Cl_2$ per tubulin dimer (when it was in the polymerized state).[31]

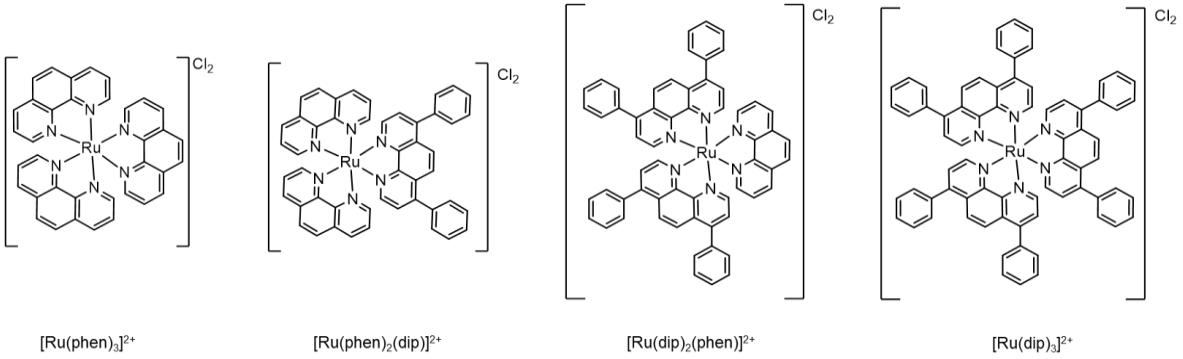

Figure 2.1. The family of Ru(II) polypyridyl complexes where the tris-phen complex's ligand is systematically altered with dip ligands until the tris-dip complex is obtained.

In this chapter, we describe our efforts to reduce the lipophilicity $[Ru(dip)_3]Cl_2$ by systematically replacing dip ligands with phen ligands. We aim to explore how this structural change will: (i) reduced the logP value, (ii) alter the cytotoxicity, (iii) affect the tubulin binding and MSA activity, and (iv) eventually screen how this changes the animal toxicity. The $logP_{o/w}$ and typical IC_{50} for $[Ru(phen)_3]Cl_2$ are -1.5 and >50 µM respectively, whereas for $[Ru(dip)_3]Cl_2$ are 1.9 and ~3 uM, respectively. Cellular uptake studies reveal that $[Ru(dip)_3]Cl_2$ is taken up more by cells at about a 7-fold increase than $[Ru(phen)_3]Cl_2$, suggesting uptake is the primary reason for their difference in cytotoxicity.

The synthesis of the two RPCs intermediates; $[Ru(dip)(phen)_2]Cl_2$ and $[Ru(dip)_2(phen)]Cl_2$ is described and the complete family of RPCs under investigation are shown in Figure 2.1.

2.2 Experimental

2.2.1 Chemicals

All reagents and solvents used were reagent grade and were used as received unless otherwise noted. Ruthenium(III) chloride trihydrate (Pressure Chemical Co),

tetrabutyl ammonium chloride hydrate, 1,10-phenanthroline (phen), 4,7-diphenyl-1,10-phenanthroline (dip), ammonium hexafluorophosphate, lithium chloride (LiCl), ethanol, methanol, acetone, acetonitrile, and octanol (Aldrich) were used as received. $[Ru(phen)_3]Cl_2$ and $[Ru(dip)_3]Cl_2$ were synthesized according to literature (spectra shown in appendix Figures A.1 and A.4, respectively).[52,53] 0.1 M phosphate buffered saline (PBS,10X) (NaCl 1.37 M; KCl 0.027 M), pH 7.4 at 25 °C, was purchased from Bio-Rad and diluted 10-fold with Millipore water to give normal PBS buffer (1X).

2.3 Characterization

2.3.1. ^{1}H NMR

^{1}H NMR spectras were obtained on a JEOL Eclipse Plus 500 MHz Spectrometer using either CD_3CN, $(CD_3)_2CO$, or $(CD_3)_2SO$ as the NMR solvent. The spectra used TMS as the standard zero ppm.

2.3.2. LC-MS

LC-MS analysis were done on a Shimadzu UFLCXR (LC-20AD XR prominence pump and SIL-20AC XR prominence autosampler) with a LC-MS 2020. The parameters were as follows; no column, injection volume (1 µL), flow rate (0.25 mL/min), and runtime (2 minutes), mobile phase (100% acetonitrile), scan mode (150-1500 m/z), scan speed (1500 u/sec). All samples were dissolved in acetonitrile. Pre and post run analyses used either $[Ru(phen)_3]Cl_2$ or $[Ru(dip)_3]Cl_2$ as standards for instrument operation.

2.3.3. X-ray Crystallography

Single crystal X-ray diffraction study was carried out on a Bruker Kappa APEX-II CCD diffractometer at 100(2) K using monochromatic Mo-Kα radiation (λ = 0.71073 Å) and a detector-to-crystal distance of 5.220 cm. A 0.09 x 0.07 x 0.03 mm orange block

was mounted on a Cryoloop with Nujol oil. Data was collected in a hemisphere or full sphere of reciprocal space with 0.3° scans in ω for an exposure time of 30 s per frame up to a maximum 2θ value of 63.1°. A total of 2834 reflections were collected covering the indices, $0 \leq h \leq 20$, $-28 \leq k \leq 27$, $0 \leq l \leq 28$. 2743 reflections were found to be symmetry independent, with a R_{int} of 0.0502. Indexing and unit cell refinement indicated a monoclinic lattice. The space group was found to be I2/c. The measured intensities were corrected for Lorenz and polarization effects and were further corrected for absorption using the multi-scan method SCALE3 ABSPACK. Based on the data, structural model was obtained by direct method using the Superflip subroutine implemented in the JANA2006 software package. The refinement was performed via full-matrix least-squares on F^2 by using the JANA2006 software package.

2.3.4 UV-Vis Spectrophotometer

All LogP values (lipophilicity determination) were measured using an Agilent 8453 UV-visible spectrophotometer and a Starna Cell Quartz spectrophotometer cuvette. Each partition was read in triplicate from 300-600 nm. Optical density measurements were recorded at 460 nm. Spectra were compared to either a $[Ru(phen)_3]Cl_2$ or $[Ru(dip)_3]Cl_2$ standard.[50] The spectra are compared to the standard spectra of the sample, the extinction coefficient derived spectra, and the optical density measurement is recorded at 460 nm.

2.4 Synthesis

2.4.1 Synthesis of $[Ru(phen)_2Cl_2]$

$Ru(phen)_2Cl_2$ was made in analogous fashion to $Ru(bpy)_2Cl_2$ reported previously in literature by Sullivan et al.[52] Briefly, $RuCl_3 \cdot xH_2O$ (0.2 g, 0.76 mmol), phen (0.51 g, 1.68 mmol), and LiCl (0.11 g, 2.6 mmol) were added to a two-neck round bottom flask with 20 mL of dimethylformamide (DMF) and refluxed under nitrogen overnight. The dark black-brown solution was transferred into a beaker and about 60 mL of acetone was added and stirred. The resulting slurry was left at -4 ˚C for 12 h. The solution was filtered cold, then the precipitate was washed with copious amounts of water and followed by acetone until the trailing was almost clear. After a final washing with diethyl ether, the precipitate was dried at 80 ˚C for 12 h. Yield 84 %. ^{1}H NMR ($(CD_3)_2SO$): 10.25 (dd, 2H), 8.67 (dd, 2 H), 8.25 (dd, 2 H), 8.16-8.21 (m, 4 H), 8.10 (dd, 2 H), 7.72 (dd, 2 H), 7.29 (dd, 2H).

2.4.2 Synthesis of $[Ru(phen)_2dip]Cl_2$

$[Ru(phen)_2dip]Cl_2$ was made using a method derived by Dwyer.[54] $[Ru(phen)_2Cl_2]$ (0.106 g, 1 mmol) and dip (0.092 g, 1 mmol) were added to a round-bottom flask containing 110 mL of 5:1 of ethanol:water and refluxed overnight. The hot solution was filtered, and the filtrate was concentrated by rotary-evaporation until the total volume was ~ 40 mL. This solution was filtered (medium porosity glass frit) to remove any solids, and the filtrate evaporated to dryness. Once dry, the resulting red/orange solid was suspended in 20 mL of dry acetone and sonicated for 10 min to dissolve any uncoordinated ligand. The red solid was collected by filtration, washed with 10 mL fresh acetone, and oven dried at 60 ˚C for 12 h. Yield 83 %. ^{1}H NMR (CD_3CN): 8.62 (m, 4H), 8.27 (s, 4H), 8.17 (dd, 2 H), 8.14 (s, 2H), 8.05 (m, 4H), 7.68 (dd, 2H), 7.64-7.53 (m, 15H); Anal. Calcd for $C_{48}H_{32}Cl_2N_6Ru$: C 61.54, H 4.30, N 8.97, found: C 58.30, H 4.39, N 8.42;

ESI-MS (m/z): 397.1 $[M\text{-}Cl_2]^{2+}$ X-ray quality crystals were obtained by slow evaporation of the concentrated product in acetonitrile, acetone, ether solution.

2.4.3 Synthesis of $[Ru(dip)_2Cl_2]$

$Ru(dip)_2Cl_2$ was made in analogous fashion to $Ru(bpy)_2Cl_2$ reported previously in literature by Sullivan et al.[52] $RuCl_3{\cdot}xH_2O$ (0.2 g, 0.76 mmol), dip (0.56 g, 1.68 mmol), LiCl (0.11 g, 2.6 mmol) were added to a two-neck round bottom flask with 20 mL dry DMF and refluxed under nitrogen overnight. The mixture was then cooled to room temperature and 30 mL of DI water was added, which resulted in precipitation. The dark purple product was collected via filtration and washed with copious amounts of water until the trailing was almost clear. 10 mL of ether was added to dry the purple product. The compound was recrystallized in acetone and water was added to obtain the precipitate. The dark purple precipitate was filtered and washed with copious amounts of water until the trailing was almost clear. After the final washing with diethyl ether, the precipitate was dried at 80 ˚C for 12 h. Yield 81%. ^{1}H NMR ($(CD_3)_2SO$): 10.40 (d, 2 H), 8.19-8.24 (dd, 4 H), 8.00 (dd, 4 H), 7.81 (t, 5 H), 7.70 (t, 4 H), 7.62 (t, 2 H), 7.47-7.57 (m, 11 H), 7.37 (d, 2 H).

2.4.4 Synthesis of $[Ru(dip)_2phen]Cl_2$

$[Ru(dip)_2phen]Cl_2$ was made using a method derived by Dwyer.[54] $[Ru(dip)_2Cl_2]$ (0.203 g, 1 mmol) and phen (0.044 g, 1 mmol) were added to a round-bottom flask containing 110 mL of 5:1 of ethanol:water and refluxed overnight. The hot solution was filtered, and the filtrate was concentrated by rotary-evaporation until the total volume was ~ 40 mL. This solution was filtered (medium porosity glass frit) to remove any solids, and the filtrate evaporated to dryness. Once dry, the resulting red/orange solid was suspended in 20 mL of dry acetone and sonicated for 10 min to dissolve any

uncoordinated ligand. The red solid was collected by filtration, washed with 10 mL fresh acetone, and oven dried at 60 ˚C for 12 h. Yield 80 %. ^{1}H NMR (CD_3CN): 8.65 (dd, 2H), 8.29 (s, 2H), 8.24 (dd, 2H), 8.21 (dd, 2H), 8.17 (s, 4H), 8.1 (d, 2H), 7.71 (dd, 2H), 7.63-7.55 (m, 44H); Anal. Calcd for $C_{60}H_{40}Cl_2N_6Ru$: C 66.17, H 4.44, N 7.72, found: C 63.87, H 4.27, N 7.16; ESI-MS (m/z): 473.1 $[M\text{-}Cl_2]^{2+}$

2.5 Experiments

2.5.1 Partition Coefficient Determinations

Partition coefficients (LogP) for each complex were determined using the shake-flask method. A complex was dissolved in equal parts octanol and water or PBS, shaken for 30 min, and left to equilibrate for 24 h during which the aqueous and octanol phases separated. The distribution between phases was determined by measuring the absorbance at 460 nm in each phase. LogP values were calculated as the decadic logarithm of the ratio of solute concentrations in both phases:

$$\log P_{o/(w \text{ or } b)} = \log \left(\frac{[\text{solute}]_{\text{octanol}}}{[\text{solute}]_{(\text{water or buffer})}}\right)$$

These data are shown in Table 2.2.

2.6 Results and Discussion

Syntheses and characterization of RPCs

The synthetic routes for preparing of $[Ru(phen)_2dip]Cl_2$ and $[Ru(dip)_2phen]Cl_2$ are shown in Scheme 1, and follow a well-established procedure for the change of the three bidentate ligands in tris chelate ruthenium(II) complexes. Initially, $Ru(L\text{-}L)_2Cl_2$ is prepared from $RuCl_3$ and two equivalents of L-L (the desired diamine ligand) and the chlorides in this complex are replaced by the second dimine ligand (L'-L'). Typically, these products

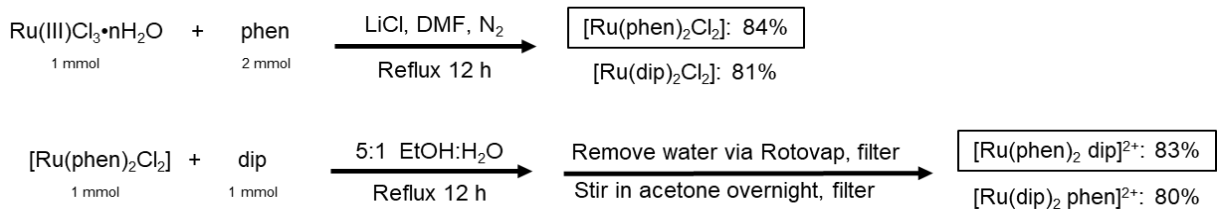

Scheme 1. The synthesis route for the preparation of $[Ru(phen)_2dip]Cl_2$. The synthesis route of $[Ru(dip)_2phen]Cl_2$ is also implied based on the starting material (top reaction) using dip instead of the phen ligand and the bottom reaction starting with $[Ru(dip)_2Cl_2]$ and using phen instead of the dip ligand. The mmol amount of each reagent is indicated as well as the percent yield calculated.

are worked up by removing the alcoholic solvent, leaving a predominantly aqueous solution of the product as the chloride salt. Selective precipitation of the product RPC with NH_4PF_6, yield for example $[Ru(phen)_2(dip)][PF_6]_2$ which is then isolated, dried, and metathesized back to the chloride salt for aqueous studies. Unfortunately, the solubility of the dip complexes makes this process untenable, as it is challenging to cleanly remove the PF_6^- counterions completely in subsequent metatheses. We opted to isolate the chloride salt directly by driving the chloride substitution reaction to completion with a 1:1 of the incoming diamine and then washing away the uncoordinated complex with acetone washes. This method cleanly yields the desired RPC, as the chloride salt in high yield.

Both $[Ru(phen)_2dip]^{2+}$ and $[Ru(dip)_2phen]^{2+}$ were characterized via ^1H NMR (Figure 2.2 and 2.3, full NMR are in appendix Figures A.2 and A.5, respectively) in deutero-acetonitrile and ESI-MS. The ^1H labeling for each heteroleptic complex was determined based on COSY (spectra shown in appendix Figures A.3 and A.6, respectively). The homoleptic complexes have a D_3 symmetry whereas altering one ligand lowers the symmetry to C_2. $[Ru(phen)_2dip]^{2+}$ is expected to show 16 unique NMR peaks whereas $[Ru(dip)_2phen]^{2+}$ should show 20 peaks. Unfortunately, the proton NMR peaks associated with the phenyl groups are closely grouped in the 7.5 to 7.6 ppm region and not easily

differentiated; thus, only 12 and 11 peaks are definitively assigned in $[Ru(phen)_2dip]^{2+}$ and $[Ru(dip)_2phen]^{2+}$, respectively.

The ESI-MS data shows parent ion peaks for each of the complexes in their divalent state without associated counterions, $[Ru(phen)_2dip]^{2+}$ or $[Ru(dip)_2phen]^{2+}$. The calculated m/z for $[Ru(phen)_2dip]^{2+}$ is 397 and 397.1 is found, whereas for $[Ru(dip)_2phen]^{2+}$ the calculated m/z is 473 and 473.1 found. The CHN analysis for both complexes were sent to Intertek. For $[Ru(phen)_2dip]Cl_2$ the analysis was calculated using $C_{48}H_{32}Cl_2N_6Ru$: C 61.54, H 4.30, N 8.97 and the found values were: C 58.30, H 4.39, N 8.42. For $[Ru(dip)_2phen]Cl_2$ the analysis was calculated using $C_{60}H_{40}Cl_2N_6Ru$: C 66.17, H 4.44, N 7.72 and the found values were: C 63.87, H 4.27, N 7.16.

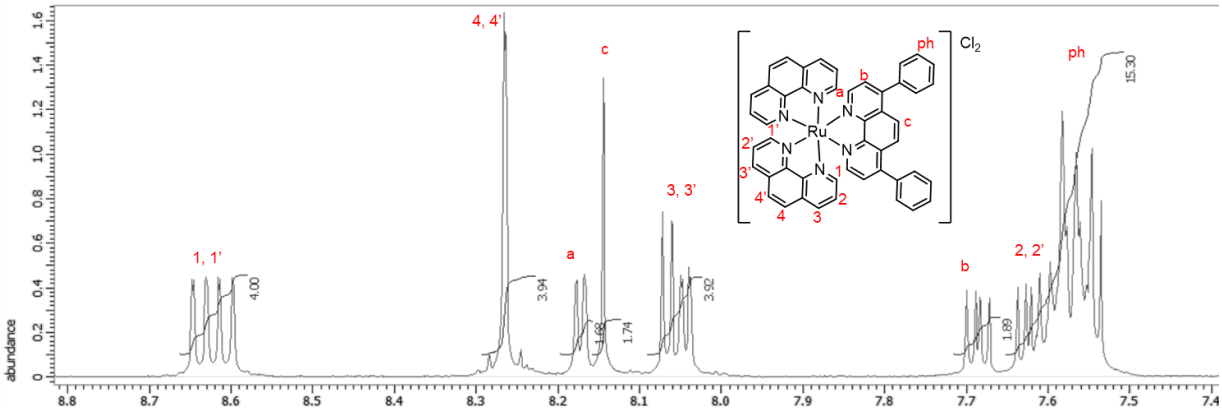

Figure 2.2. Labeled ^1H NMR of $[Ru(phen)_2dip]Cl_2$ in CD_3CN. Numbers 1-4 and 1'-4' represent the protons on the phen ligands and the letters a-c and ph refer to the protons on the dip ligand. (where ph= phenyl group)

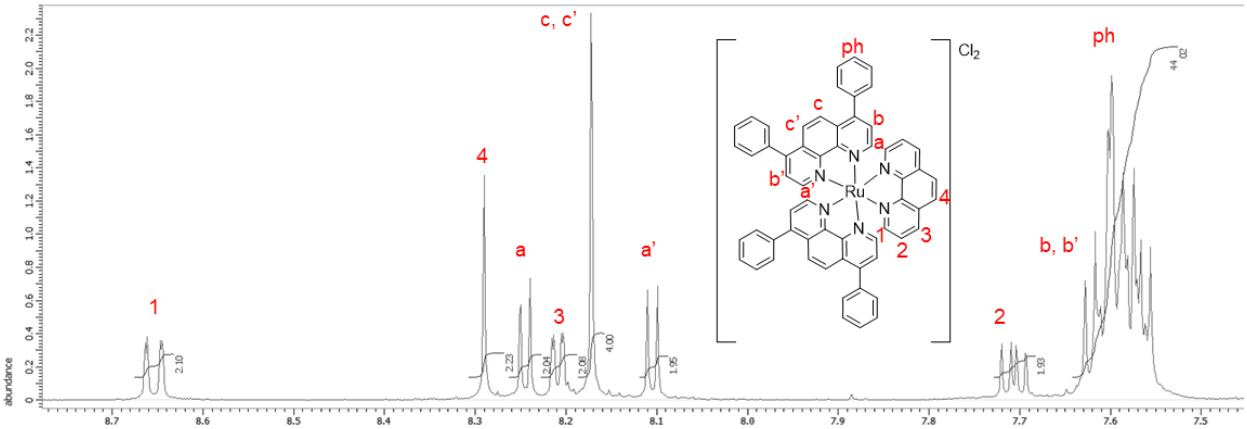

Figure 2.3. Labeled ^{1}H NMR of $[Ru(dip)_2phen]Cl_2$ in CD_3CN. Letters a-c, ph, and a'-c' refer to the protons on the dip ligands and the numbers 1-4 represent the protons on the phen ligand. (where ph= phenyl group)

X-ray quality crystals of $[Ru(phen)_2dip]^{2+}$ were obtained by slow evaporation of acetonitrile, acetone, and ether. The experimental methods for X-ray diffraction are outlined above in section 2.3.3. The analysis had to be done at low temperatures to obtain quality crystal data, most likely due to the high solubility of this complex. The crystal structure obtained is shown in Figure 2.4 and the crystallography data is summarized in Table 2.1. The atomic coordinates and displacement parameters, anisotropic atomic displacement parameters, atomic distance, and bond angles are displayed in appendix Tables 1-4.[55]

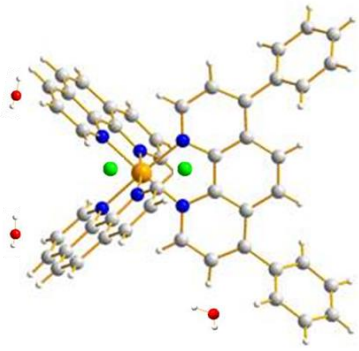

Figure 2.4. Crystal structure obtained for the $[Ru(phen)_2dip]Cl_2$ complex. Green balls indicate chloride counterions and red balls indicate waters of crystallization. Hydrogen positions are calculated.

Table 2.1. Crystal data and structure refinement.

Identification code		
Empirical formula	$C_{48}H_{40}Cl_2N_6O_4Ru_1$	
Molecular formula	$C_{48}H_{40}Cl_2N_6O_4Ru_1$	
Moiety formula	$C_{48}H_{32}N_6Ru_1$, $(Cl)_2$, $(H_2O)_4$	
Formula weight	1406.3 g/mol	
Temperature	100.0 K	
Wavelength	0.71073 Å	
Crystal system	Monoclinic	
Space group	I2/c	
Unit cell dimensions	a = 14.0102(11) Å	α= 101.31(3) °
	b = 19.1218(13) Å	β= 90 °
	c = 19.2037(12) Å	γ = 90 °
Volume	5044.768() $Å^3$	
Z	4	
Density (calculated)	1.2336 g/cm^3	
Absorption coefficient	0.467 mm^{-1}	
F(000)	1920	
Crystal size	0.09 x 0.07 x 0.03 mm^3	
Crystal color, habit	Orange block	
Theta range for data collection	2.51 to 31.55°	
Index ranges	-0≤h≤20, -28≤k ≤27, 0≤l≤28	
Reflections collected	2834	
Independent reflections	2743 [R(int) = 5.02 %, R(sigma) = 3.71%]	
Completeness to theta = 31.55°	98%	
Absorption correction	multi-scan	
Max. and min. transmission	0.960 and 0.987	
Refinement method	Full-matrix least-squares on F^2	
Data / restraints / parameters	2743/0/258	
Goodness-of-fit on F^2	1.47	
Final R indices [I>3sigma(I)]	R1 = 5.02, wR2 = 3.71	
R indices (all data)	R1 = 5.02, wR2 = 3.71	
Extinction coefficient	n/a	
Largest diff. peak and hole	- 0.05 and + 0.05 e^- $Å^{-3}$	

Lipophilicity studies

The lipophilicity of these complexes was quantified by measuring the partition coefficient between two immiscible solvents, octanol and water ($LogP_{o/w}$) or octanol and buffer mixtures ($LogP_{o/b}$), via the shake-flask method outlined in experimental 2.51. Although the LogP data for both o/w and o/b in Table 2.2 mirror each other, differences between the water and the buffer used in this experiment is valuable. The $LogP_{o/w}$ are typically more negative since the buffered system can have salting out effects. Since we are trying to correlate uptake within the cell to lipophilicity, the $LogP_{o/b}$ obtained in octanol/PBS is generally going to present the most realistic model than the $LogP_{o/w}$. LogP values that are positive, and typically greater than ~1.5 show poor solubility in polar protic solvents, whereas LogP values that are negative show greater solubility in polar protic solvents.[50,56,57] In general, both tested systems follow the same trend between each of the complexes: the more dip ligands present, the more lipophilic the complex; $[Ru(phen)_3]Cl_2$ < $[Ru(phen)_2dip]Cl_2$ < $Ru(dip)_2phen]Cl_2$ < $[Ru(dip)_3]Cl_2$. The results observed follow the hypothesized trend, and complexes $[Ru(phen)_3]Cl_2$, $[Ru(phen)_2dip]Cl_2$, and $Ru(dip)_2phen]Cl_2$ are readily soluble in water. By just changing one of the ligands on $[Ru(phen)_3]Cl_2$ complex to a dip ligand, the LogP value changed from -1.1 to 1.2 which indicates the lipophilic properties this ligand creates. These results agree with Barton et al., MacDonnell, and many others where the dip-based complexes show a much higher lipophilicity than the phen containing complexes.[24,51,58]

Table 2.2. LogP values in octanol/buffer (o/b) and octanol/water (o/w) the studied compounds.

Complex	$LogP_{o/b}$	$LogP_{o/w}$
$[Ru(phen)_3]Cl_2$	-1.1	-1.5
$[Ru(phen)_2dip]Cl_2$	1.2	-1.1
$[Ru(dip)_2phen]Cl_2$	1.6	0.3
$[Ru(dip)_3]Cl_2$	1.9	1.4

2.7 Conclusion

In this chapter we have synthesized and characterized 4 complexes which will begin a mini structure activity relationship evaluated in Chapter 3. This family of RPCs vary by altering the ancillary ligands from dip to phen. The difference between the two ligands (phen and dip) is the di-phenyl substituents on the dip ligand. After characterization by H^1 NMR, ESI-MS, and CHN the family of complexes were evaluated for their lipophilic properties. It was seen that as the number of dip ligands increased, so did the lipophilicity. By alternating one of the ligands on the complex $[Ru(phen)_3]Cl_2$ to a dip ligand ($[Ru(phen)_2dip]Cl_2$), the LogP value changed from hydrophilic to lipophilic ($LogP_{o/b}$ -1.1 to 1.2, for $[Ru(phen)_3]Cl_2$ and $[Ru(phen)_2dip]Cl_2$ respectively). This indicates the strong lipophilic properties this dip ligand creates. Whereas, when altering one of the ligands on the complex $[Ru(dip)_3]Cl_2$ to a phen ligand ($[Ru(dip)_2phen]Cl_2$), this complex's solubility is enhanced (now soluble in water). This indicates the hydrophilic properties enhanced just one phen ligand creates. Clearly, as many studies have shown before, ancillary ligands have a major impact on a complex's lipophilicity.[59–61]

CHAPTER 3

Investigations of the Cellular Uptake, Cytotoxicity, and Microtubule Stabilizing Activity of Ru(II) Polypyridyl Complexes Containing One, Two, or Three Diphenylphenanthroline Ligands

3.1 Introduction

The lipophilicity of an anti-cancer agent has a major impact on a drugs bioavailability, rate of absorption into the bloodstream, the amount of cellular uptake, and in many cases the strength of binding to its cellular target.[21,57] Zava et al. examined the cytotoxicity of homoleptic RPCs ($[Ru(bpy)_3]^{2+}$, Ru(N^4,N^4,$N^{4'}$,$N^{4'}$-tetraethyl-[2,2'-bipyridine]-4,4'-diamine)$_3]^{2+}$, Ru(dimethyl [2,2'-bipyridine]-4,4'-dicarboxylate)$_3]^{2+}$, $[Ru(4,4'\text{-dimethoxy-}2,2'\text{-bipyridine})_3]^{2+}$, and $[Ru(4,4'\text{-dimethyl-}2,2'\text{-bipyridine})_3]^{2+}$ on A2780 ovarian cancer cells. They reported that the most cytotoxic of these complexes, $[Ru(4,4'\text{-dimethoxy-}2,2'\text{-bipyridine})_3]^{2+}$ (<1 μM), was also lipophilic ($LogP_{o/w}$= 0.55). Interestingly, this complex appeared to target the plasma membrane rather than the common target, DNA.[62] In addition, Pisani et al. described this behavior in binuclear RPCs in which cellular uptake and localization were determined using flow cytometry. Overall, the study suggested that cytotoxicity corresponds to the lipophilic behavior and can be altered by changing the coordinated ligand. These complexes were also seen to mainly localize within the mitochondria.[59] These two studies, and many more, indicate the strength an ancillary ligand's lipophilicity has on cytotoxicity and uptake.

In order for promising complexes to emerge, quick screening tool(s) are necessary, such as lipophilicity and cytotoxicity. Promising complexes are evaluated for their uptake and sub-cellular localization to better understand where the complex enters the cell,

where the complex is localizing, and potentially where the complex is causing cytotoxic effects. It has been postulated by other scientists that obtaining a new therapeutic target may overcome the current issues with cisplatin resistance. Therefore, there is a need to develop new anticancer drug classes with a different mechanisms of action.[7,13,15,18,37,63]

This project investigates Ru-based metallodrugs that are similar to the $[Ru(dip)_3]^{2+}$ complex (findings of $[Ru(dip)_3]^{2+}$ detailed in Chapter 1) that potentially localize mainly in the cytoskeleton and exert their anticancer effects by interfering with microtubule (MT) function.[31] MTs are highly dynamic polymers of tubulin, which are crucial in maintaining the structure of the cell and are involved in processes critical to cell survival (e.g., intracellular transport and cell division). Therefore, MTs represent an attractive target for anticancer therapy. Drugs that target MTs are known as microtubule targeting agents (MTAs). Paclitaxel, Docetaxel (DTX), and Vinorelbine (Figure 3.1) are among the only FDA-approved MTAs for cancer treatment. These organic natural products, or semi-synthetic natural products, are used to treat a variety of cancers but exhibit dose-limiting toxicity, are susceptible to resistance over time, and can require excipients. In addition, the supply of some of these natural products is limited and synthetic routes for their preparation can exceed 40 steps.[31,35,37,63–66] Two Ru-based metallodrugs have been investigated in human clinical trials for cytotoxic cancer therapy; none were clinically approved, and they do not act as MTAs.[17]

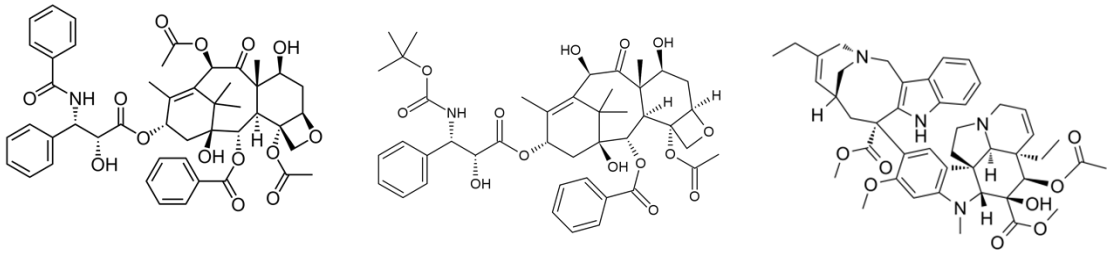

Figure 3.1. Among the FDA approve organic based microtubule targeting agents.[16,35,67]

In chapter 2, $[Ru(dip)_3]Cl_2$ was altered systematically with phen ligands to form $[Ru(phen)_2dip]Cl_2$ and $[Ru(dip)_2phen]Cl_2$ complexes. Once the complexes were structurally characterized, we determined their solubility and lipophilicity, measured as the logP. Herein, we investigate the cytotoxicity of these RPCs and compare this with the two homoleptic RPCs $[Ru(dip)_3]Cl_2$ and $[Ru(phen)_3]Cl_2$. Moreover, we have determined the extent of cellular uptake and the subcellular localization in MCF7 and H358 cell lines using ICP-MS analysis of the Ru content. Finally, the ability of these RPCs to bind and alter microtubule dynamics were analyzed using a tubulin polymerization assay.

3.2 Experimental

3.2.1 Chemicals

$[Ru(phen)_3]Cl_2$, $[Ru(phen)_2dip]Cl_2$, $Ru(dip)_2phen]Cl_2$ and $[Ru(dip)_3]Cl_2$ were prepared as described in Chapter 2. Millipore water was used to prepare all buffers. Phosphate buffered saline (PBS, 10X) was purchased from Bio-Rad and is 0.1 M phosphate buffered saline (NaCl 1.37 M; KCl 0.027 M); pH 7.4, at 25 °C. The PBS was diluted 10-fold with Millipore water to give normal PBS buffer (1X). Dimethyl sulfoxide (DMSO) and octanol was used as received from Sigma Aldrich. RPMI-1640 medium, DMEM-low glucose medium, fetal bovine serum (FBS), Trypan blue solution, sodium

bicarbonate, trypsin-EDTA (1X), 1.1 % penicillin/streptomycin, and 10X RIPA buffer was also purchased from Sigma. The Bicinchoninic acid (BCA) assay used the PierceTM BCA Protein Assay Kit (Cat: 23255) from ThermoFisher. The sub-cellular localization Qproteome Cell Compartment Kit was purchased from Qiagen (Cat: 37502). The tubulin and tubulin polymerization kit were purchased from Cytoskeleton (Cat: BK006P).

3.3 Cell Lines and Cultures

The cell line H358 (human non-small cell lung cancer-bronchioalveolar) and MCF-7 (human breast cancer) were obtained from the NCI-Frederick Cancer DCTD Tumor/Cell Line Repository by Dr. Gazdar (NCI-H358M). The H358 cells were cultured in RPMI-1640 medium whereas the MCF-7 were cultured in DMEM-low glucose each with 10 % Fetal Bovine Serum, 1 % penicillin at 37 °C in a humidified atmosphere of 5 % CO_2.

3.4 Instrumentation

3.4.1 UV-Vis Plate Reader

All MTT assays (cytotoxicity evaluation) were evaluated using a SPECTROstar Nano Microplate UV/VIS from BMG Labtech. The parameters were: 560 nm, automatic path length correction using 100 µL, no shaking. The data were exported into Excel for work-up.[68]

All BCA assays were evaluated using a SPECTROstar Nano Microplate UV/VIS from BMG Labtech. The parameters were: 562 nm, automatic path length correction using 200 µL, no shaking. The data were exported into Excel and protein concentrations were determined by linear regression from a preexisting calibration curve made using bovine serum albumin (BSA).[69]

All tubulin polymerization assays were evaluated using a SPECTROstar Nano Microplate UV/VIS from BMG Labtech. The parameters for UV-Vis were made on kinetic mode: 340 nm, constant temperature 37 °C, positioning delay 0.4, No. kinetic window 1, No. cycles 61, measurement start time 0.0 min, 20 flashes per well and cycle, automatic path-length correction using volume 110 µL, length 6.91 mm, cycle time 60 min, shaking only before first reading, no pauses between cycles, no replicates, and blank corrected was used. The data were exported to Excel for work-up. [31,38]

3.4.2 Microwave Digestion Oven

Cell samples to be analyzed for RPC (Ru content) uptake and sub-cellular fractions were digested in acid prior to ICP-MS analysis. In a typical procedure, the sample was suspended in 0.5 mL water and mixed with 5 mL 3.5 % nitric acid in a Teflon-lined microwave digestion vessel (max pressure 40 psi). The digestion vessels were placed in a Mars5 XP-1500 digestion oven and irradiated at 600 W (100 % power). The instrument was set to ramp to 130 ˚C in 5 minutes (~22 ˚C/min), then hold at this temperature for 5 minutes. The samples were cooled to room temperature before opening, the contents were transferred to a 15 mL storage tube, then their volumes were made up to 10.0 mL with 3.5 % nitric acid. There was an instrument control vessel which monitored the pressure and temperature inside the vessel to ensure set parameters were met. The vessels contained a membrane, which were changed after each run.[31,68]

3.4.3 ICP-MS

Cell samples to be analyzed for RPC (Ru content) uptake and sub-cellular fractions after digested in acid were analyzed using ICP-MS. Data was obtained using an Agilent 7700 Series ICP-MS (single quadruple) fitted with an ASX-520 CETAC autosampler, and

the data were analyzed using MassHunter Workstation Software (version B.01.01). Typical operational parameters for the ICP–MS were RF power 1400 W, Argon gas (cooling 13.0 L/min, auxiliary 0.8 L/min, nebulizer 0.8 L/min), spray chamber temperature 3 ˚C, Interface cones Nickel, Expansion chamber pressure 1.9 mbar, analyzer chamber pressure $3.6X10^{-7}$ mbar, sampling depth 150 mm, detector mode (pulse counting), standard resolution, element monitored (^{101}Ru), and integration time/mass 170 ms. Ru concentrations were established from a 5-point calibration curve using Ru standards ranging up to 128 ppb. Good linearity (R^2 >0.998) was routinely obtained under these conditions. Each concentration was measured three times and data were reported as averages and standard deviations.[31,68]

3.4.4 UV-Vis Spectrophotometer

All Ru concentrations for binding studies were measured using an Agilent 8453 UV-visible spectrophotometer and a Starna Cell Quartz spectrophotometer cuvette. Each sample was read in triplicate at 460 nm. Analyte spectra were compared to standard spectra; extinction coefficient derived spectra and optical density measurement were recorded at 460 nm.

3.5 Experiments

3.5.1 Cytotoxicity

The cytotoxicity of a given RPC was determined using an MTT (MTT= (3-(4,5-Dimethylthiazol-2-yl)-2,5-diphenyltetrazolium bromide)) indicator assay. Under normal growth conditions, viable cells uptake MTT and convert it to formazan, whereas dead cells do not affect this transformation. The formazan often crystallizes from the solution, but the addition of DMSO solubilizes this product yielding a purple solution. The concentration

of viable cells is determined optically by measuring the absorbance at 560 nm. The intensity of the formazan is directly proportional to the viable cell concentration. In a typical MTT assay, $1X10^4$ cells are loaded per well in a 96 well-plate and allowed to grow for 24 h at 37°C in a humidified atmosphere of 5 % CO_2. Cultured cells were then treated with different concentrations of the compound under analysis, typically 0.01, 0.1, 1.0, 10, and 100 μM, whereas the control and blank wells were treated with DMSO (less than 1 % v/v DMSO). The well-plate was then incubated at 37 °C for 96 h. To measure the viable cell concentration, cells were treated with 30 μL of 5 mg/mL MTT and incubated for 4 h, after which the media was removed with suction and 100 μL DMSO added to each well. The plates were gently shaken on an end-over-end shaker for 1 h prior to reading the absorbance of each well at 560 nm. The IC_{50} values were calculated from sigmoidal fits of the dose-response curves (OD vs complex concentration). IC_{50} values ≤10 μM will be interpreted as cytotoxic. This assay was performed in quintuplicate, and the standard deviations are indicated in Table 3.1.[50,68]

3.5.2 Cellular Uptake

Cellular uptake will be determined to identify the quantity of the complex that enters the cell. Briefly, 2 million MCF-7 or H358 cells were seeded on 60-mm plates, incubated for 24 h, then treated with 2 mM stock solution of the compound (final concentration 20 μM) or control (less than 1 % v/v DMSO). The cells were incubated for 1 h at 37 °C, then the media was removed, cells washed with PBS (five times), trypsinized, and centrifuged for 5 min. The pellet was washed with PBS, then resuspended (three times). Cell samples were then split into two fractions for separate analysis of Ru content using ICP-MS and cell number using BCA, then reported as ng of Ru per million cells.[31,68]

3.5.3 Bicinchoninic Acid (BCA)

BCA was used to determine the cell number in the uptake experiment, as well as determine the protein content in the tubulin stoichiometry binding assay. The BCA kit provided a reagent A and B. Reagent A contains sodium carbonate, sodium bicarbonate, bicinchoninic acid and sodium tartrate in 0.1 M sodium hydroxide, whereas the reagent B contains 4% cupric sulfate. The BCA assay works by detecting the reduction of Cu^{2+} to Cu^{1+} by protein (peptides with 3 or more amino acid residues) in a medium (that is alkaline) forming a complex with the cupric ions that is light blue. Once this occurs, a chelation of two BCA molecules with one cuprous ion occurs; this is mainly influenced by the cysteine, tyrosine, and tryptophan amino acids. When this reaction takes place, it is reflected by the change from light blue to purple color. Analysis of protein concentration is done first by using 10X RIPA buffer to lysis the cells. The pellet is resuspended in 100 µL, vortexed, sonicated, and left on ice for 30 min. 40 µL of the suspension was placed into another labelled tube. A solution of a 50:1 reagent A:reagent B from the kit was made, and 360 µL of this solution was added to the new cell suspension tube; total volume of 400 µL. The tubes were then vortexed to create a homogeneous solution. 200 µL was placed on in a covered 96-well plate that was then incubated at 37 °C for 30 min. The plate was then read using a Microplate UV-VIS spectrophotometer at 562 nm, and concentrations were determined with a preexisting calibration curve made using bovine serum albumin (BSA).[69]

3.5.4 Sub-cellular Fractionation

The localization of these RPCs is vital to obtain an understanding or their mechanism of action. This assay uses a commercial Qproteome cell compartment kit

(Qiagen, Germany) that separates the cell into 4 fractions (cytosol, mitochondria/Golgi/ER, nuclear proteins, and cytoskeleton) using a variety of buffers and temperatures which are able to interact with, and extract, each fraction. Briefly, 5 million MCF-7 or H358 cells were seeded on 60-mm plates and incubated for 12 h at 37 °C. After 24 h cells were treated with 2 mM stock solution of the compound (final concentration 20 μM) or control (less than 1 % v/v DMSO). After 1 h the media was removed, cells washed with PBS (five times), trypsinized, and centrifuged for 5 min. The pellet was washed with ice cold PBS (three times) and the cells were fractionated into 4 fractions via the Qproteome kit. The separated fractions were analyzed for Ru content (ng) by ICP-MS.[31]

3.5.5 Tubulin Polymerization Assay

MT are one of the most abundant and longest cellular protein in the cytoskeleton. MTs are made up of repeating tubulin heterodimers (α and β subunits) and have a dynamic structure; being able to grow (polymerization/stabilization known as microtubule stabilization agents, MSA) and shrink (depolymerization/destabilization known as microtubule destabilization agents, MDA). To determine if these complexes affect MT dynamics similarly to $[Ru(dip)_3]Cl_2$, a tubulin polymerization assay was performed based on methods from Cytoskeleton. This assay utilized the turbidity in the sample, that occurs from MT polymerization, to compare a natural polymerization data curve vs what occurs when an additive is used. It was seen previously that the curve for $[Ru(dip)_3]Cl_2$ was shifted above the control (which readily polymerizes at 37 ˚C) and was close to the known MSA, paclitaxel (PTX). This is suggestive that this complex interacts with MT as an MSA. Briefly, the microplate reader was set up with the parameters outlined above (section 3.4.2). On a pre-warmed (37 °C) half-area plate general tubulin buffer (GTB; 80 mM

PIPES, pH 6.9, 2mM $MgCl_2$, and 0.5 mM EGTA), used as control, alongside each 0.1 mM compound in GTB (including for refence the known MSA, PTX) were run in triplicate. The tubulin stock was diluted with tubulin polymerization buffer (TPB; 80 mM PIPES, pH 6.9, 2mM $MgCl_2$, 0.5 mM EGTA, 15 % glycerol in general tubulin buffer, and 1 mM GTP) and rapidly added to sample wells. Another tubulin polymerization assay was done in the presence of Albumin (BSA), to determine if BSA affected the polymerization of tubulin in the presence of these RPCs. This experiment was done in triplicate, but the standard deviations are not displayed on Figures 3.4 and 3.5 for clarity.[31,38]

3.5.6 Tubulin Stoichiometry Binding Assay

The tubulin stoichiometry binding assay was created based on the knowledge that tubulin readily polymerizes at 37 ˚C into microtubules and polymerized tubulin (microtubules) are able to be pelleted and separated from unpolymerized tubulin.[70] This assay was developed with a combined strategy of the tubulin polymerization assay and a modified version of the microtubule-pelleted assay by Murphy et al.[38,70] The addition of bovine serum albumin (BSA) was used to aid in non-specific binding.[71,72] A tubulin polymerization assay was done to ensure polymerization was not greatly affected in the presence of BSA (assay discussed 3.5.6 and results in Figure 3.5). First, an 80 µM of Ru complex stock was made in general tubulin buffer (GTB) from cytoskeleton (using a 5 mM stock of Ru complex in DMSO). 200 µL of this 80 µM stock was then added to a 1.5 mL microcentrifuge tube labeled C (C: BSA and Ru complex). Next, an 800 µM BSA stock in GTB was prepared. 200 µL of this 800 µM stock was added to a 1.5 mL microcentrifuge tube labeled B and C (B: tubulin and BSA). To ensure all samples had equal volumes of 400 µL, 200 µL of GTB was added to 1.5 mL microcentrifuge tubes labeled A and B.

Lastly, prepared 1 mg/mL tubulin (9.9 µM) from cytoskeleton was diluted into a 19.8 µM stock solution using tubulin polymerization buffer (buffer described above 3.5.6). 200 µL of this tubulin stock was placed in both A and B labeled 1.5 mL microcentrifuge tube (A: tubulin control). Therefore, in total this experiment had 3 samples with equal 400 µL volume, tubulin concentration (if present), BSA concentration (if present) and Ru complex (if present); A; tubulin control, B; tubulin and BSA, and C; BSA and Ru complex.

Each of these tubes were slightly mixed via a 'flicking' motion and allowed to polymerize in the incubator (37 ˚C) for 1 h. After 1 h the samples were centrifuged at 13,000 rpm for 30 min at 37 ˚C. Then, the supernatant was removed (free Ru and unpolymerized tubulin) and the pellet (bound Ru to polymerized tubulin, microtubule) was left unagitated. In order to solubilize the pellet, it was resuspended using 10X RIPA buffer, vortexed, sonicated, and left on ice for 30 min. After 30 min the remaining pellet was mixed with a pipette and sonicated on ice for about 1-1.5 h. Once the sample was fully homogeneous, each sample was split into two fractions; analysis of protein concentration (BCA and calibration curve described in section 3.5.4) and Ru analysis (determined using an UV-visible spectrophotometer and the complex's extinction coefficient (ε) using Beer's Law, $A=\varepsilon*c*l$, where ε for $Ru(dip)_2phen]Cl_2$ was predetermined to be 20,300 in water, PBS, and GTB, described in section 3.4.1). This experiment was performed in triplicate and the standard deviations are displayed in Table 3.3.

3.6 Results and Discussion

As shown in Table 3.1, the lipophilicity of the four RPCs increases as we sequentially replace phen ligands with dip ligands in the basic $[Ru(L\text{-}L)_3]^{2+}$ complex cation. The largest change in the logP for the octanol/buffer system is seen between

$[Ru(phen)_3]Cl_2$ (-1.1) and $[Ru(phen)_2dip]Cl_2$ (1.2) and subsequent replacements lead to modest further increases in $LogP_{o/b}$ with 1.6 for $[Ru(dip)_2phen]Cl_2$ and 1.9 for $[Ru(dip)_3]Cl_2$. Since the buffer used is phosphate buffered saline (PBS, 137 mM NaCl, pH 7.2), there is an excess of chloride ions present to accompany the complex cation into the non-polar phase. Moreover, the solvated ions in the aqueous phase act to 'salt out' or further push less-polar compounds into the octanol phase. While $[Ru(phen)_3]Cl_2$ is quite hydrophilic in buffer ($logP_{o/b}$ -1.1), in octanol/water mixtures, the logP is even more negative at -1.5. Interestingly, in the octanol/water system, the $logP_{o/w}$ changes substantially between two different RPCs, namely $[Ru(phen)_2dip]Cl_2$ (-1.1) and $[Ru(dip)_2phen]Cl_2$ (0.3), suggesting a different distribution of polar/non-polar complexes. Given the disparities between the octanol/buffer and octanol/water systems it is curious as to which better represent the cellular milieu.

When assayed for cytotoxicity, we observe that all the RPCs are reasonably cytotoxic with IC_{50} <10 uM, except $[Ru(phen)_3]Cl_2$ with values in excess of 50 uM. Given the large break seen in the $logP_{o/b}$ data at this point, it appears that this partition coefficient data correlates well with the cytotoxicity data, however actual measurements of the Ru content in treated MCF7 or H358 cells reveal the picture is not quite so clear cut. As shown in Figure 3.2, we observe a gradual rise in the intracellular Ru content as we progress from least lipophilic to most lipophilic, which ultimately range from 5 ng Ru/million cells to 123 ng Ru /million cells. The biggest jump in uptake is seen between $[Ru(phen)_2dip]Cl_2$ (~25 ng Ru /million cells) and $[Ru(dip)_2phen]Cl_2$ (~85 ng Ru /million cells), and which is arguably, in better agreement with the $logP_{o/w}$ data. We can rationalize these finding by assuming that the more lipophilic complexes not only better enter the

cells but, in addition, are also more potent cytotoxins. This trend agrees with many of the complexes the MacDonnell lab investigated, and many others, where the dip-based complexes show a much higher cytotoxicity than the phen containing complexes.[24,73]

Table 3.1. Outlined data obtained from the cytotoxicity (H358 and MCF-7) of the studied compounds. The LogP values in octanol/buffer (o/b) and octanol/water (o/w) are also outlined for comparison.

Complex	$LogP_{o/b}$	$LogP_{o/w}$	$H358_{IC50}$	$MCF\text{-}7_{IC50}$
$[Ru(phen)_3]Cl_2$	-1.1	-1.5	>50 μM	>50 μM
$[Ru(phen)_2dip]Cl_2$	1.2	-1.1	7.0 μM ± 0.3	9.6 μM ± 0.4
$[Ru(dip)_2phen]Cl_2$	1.6	0.3	3.5 μM ± 0.4	1.2 μM ± 0.2
$[Ru(dip)_3]Cl_2$	1.9	1.4	1.7 μM ± 0.2	1.5 μM ± 0.3

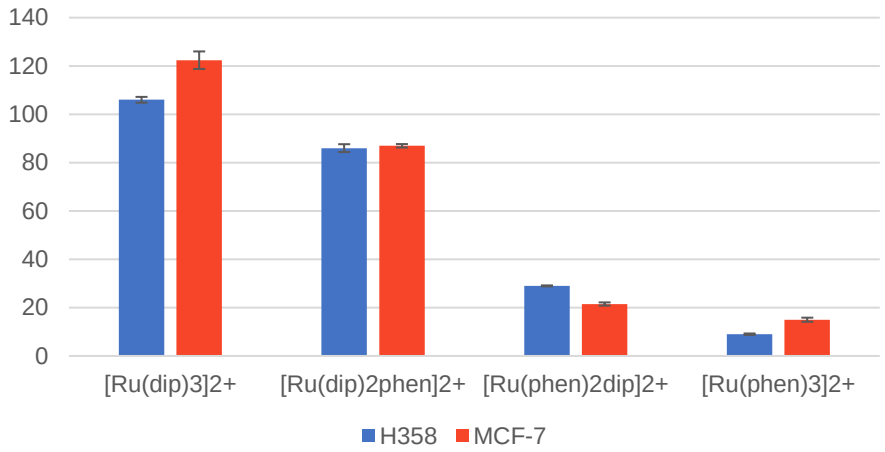

Figure 3.2. Uptake data on both H358 (blue) and MCF-7 (red) cell lines at 37 ˚C of Ru content from the treated family of compounds. The mass of Ru is displayed in ng per million cells that were treated with 20 μM and incubated for 1 h at 37 ˚C which was determined via ICP-MS.

Sub-cellular uptake

The cellular target of these RPCs, especially $[Ru(dip)_3]Cl_2$, is controversial with some groups supporting the mitochondria and our recent report on the targeting of the cytoskeletal proteins, notably tubulin.[28,31] The two targets are not mutually exclusive, and it may well be that both are targeted to different extents in differing cell lines. Most

subcellular localization studies rely of fluorescent microscopy with the inherent red luminescence of $[Ru(dip)_3]Cl_2$ imaged and being shown to localize with organelle specific dyes such as Mitotracker Green.[28] While this is a reasonable approach it will tend to highlight regions of high concentration and assumes similar luminescent quantum yield regardless of the local environment. We explored an alternative approach in which treated cells were fractionated into four distinct proteinaceous components using a well-known protocol.[74] Once isolated these components were digested and analyzed for absolute Ru content using ICP-MS.[31]

The subcellular localization data are shown using bar graphs in Figure 3.3 and 3.4 for MCF7 and H358 cell lines, respectively. The absolute amount of Ru, reported as nanograms (ng) of Ru per 1 million cells, in each of the four fractions are given. The fractions are color coded and listed left to right are, the cytoplasmic proteins (blue), the mitochondria, Golgi apparatus and ER proteins (red), the nuclear proteins (green), and the cytoskeletal proteins (purple). The two most hydrophilic and least uptaken RPCs, $[Ru(phen)_3]Cl_2$ and $[Ru(phen)_2dip]Cl_2$ show the most uniform distribution, with the largest amount being found in the mitochondria/Golgi/ER fraction. The bar graphs for the two most lipophilic complexes, $[Ru(dip)_2phen]Cl_2$ and $[Ru(dip)_3]Cl_2$ reveal a sudden and dramatic shift to localization in the cytoskeletal fraction, with over 90% of the total Ru localized there for $[Ru(dip)_3]Cl_2$ and ~65% there for $[Ru(dip)_2phen]Cl_2$. Notably, the bulk (~28%) of the remaining intracellular ruthenium in $[Ru(dip)_2phen]Cl_2$ is found in the mitochondrial fraction. The dramatic increase in cytoskeletal localization correlates with the increased Ru uptake and the observed increase in cytotoxicity, as collectively these two RPCs have IC_{50} <3.5 uM for the two cell lines examined.

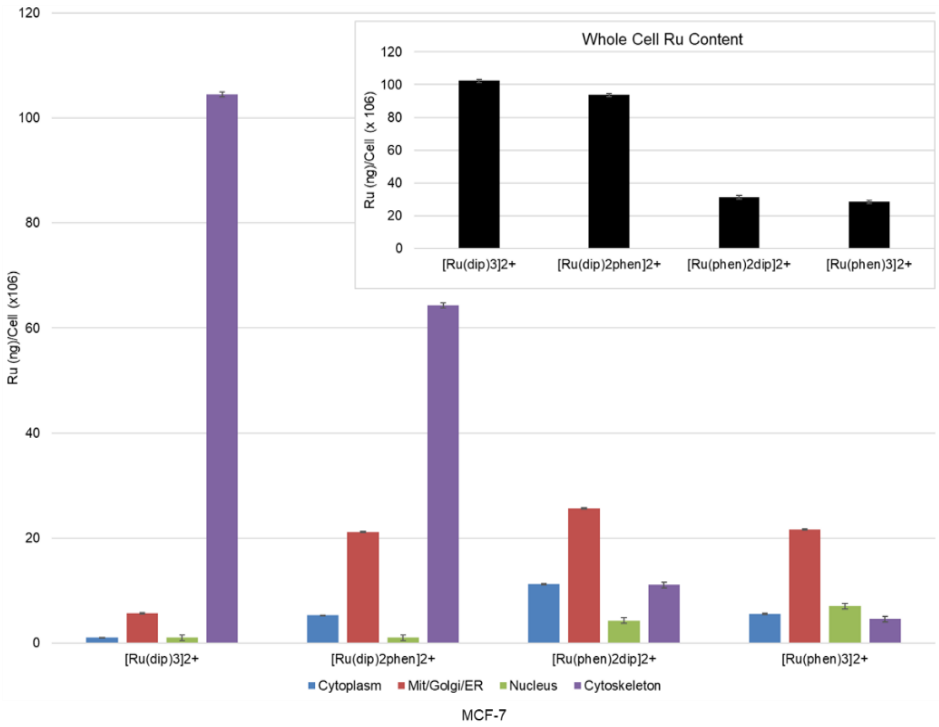

Figure 3.3. Sub-cellular localization data of and MCF-7 cell line at 37 ˚C of Ru content from the treated family of compounds. The Ru (reported as ng per million cells) found in each of the four fractions (nucleus, cytosol, mitochondria/Golgi/ER, cytoskeleton) using QIAGEN compartment kit and Ru ion content analyzed using ICP-MS. In set shows the total Ru mass for each cell and is report as ng per million cells.

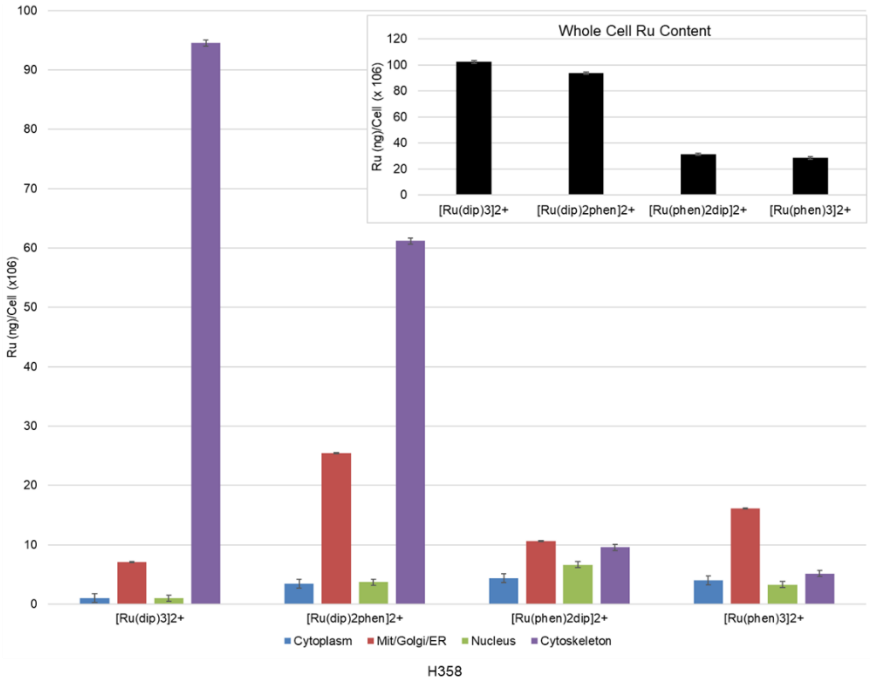

Figure 3.4. Sub-cellular localization data of and H358 cell line at 37 ˚C of Ru content from the treated family of compounds. The Ru (reported as ng per million cells) found in each of the four fractions (nucleus, cytosol, mitochondria/Golgi/ER, cytoskeleton) using QIAGEN compartment kit and Ru ion content analyzed using ICP-MS. In set shows the total Ru mass for each cell and is report as ng per million cells.

Tubulin polymerization assay

Our prior work with $[Ru(dip)_3]Cl_2$ revealed tight binding to tubulin and microtubule stabilizing activity both *in vitro* and in live cells.[31] Microtubule stabilizing agents (MSAs) are generally observed to be potent cytotoxins and are an important class of clinically used anti-cancer drugs.[35,43,75–77] Our 2020 publication of the MSA activity of $[Ru(dip)_3]Cl_2$ also revealed that even $[Ru(phen)_3]Cl_2$ has MSA activity *in vitro*, albeit less potent than the dip complex.[31] The *in vitro* tubulin polymerization assay was performed to determine the effect these RPCs have on the polymerization of tubulin. It is known that at 4 ˚C tubulin (αβ heterodimer) is in its' unpolymerized form and once the temperature is increase to 37 ˚C tubulin readily polymerizes to form MT. In Figure 3.5, a control polymerization curve (light blue) with no RPC added serves as the control and the black curve showing the behavior in the presence of a well-known MSA, paclitaxel (PTX). The subsequent runs reveal the effects of added RPC at 10 uM and it is seen that all the resulting RPC curves fall between the control and the PTX curve, indicating varying degrees of MSA activity. If we correlate MSA activity with the position of the curves, in comparison with the PTX and control curves, we observe the following trends in MSA activity: PTX>> $[Ru(dip)_2phen]Cl_2$ > $[Ru(dip)_3]Cl_2$ > $[Ru(phen)_3]Cl_2$ ~ $[Ru(phen)_2dip]Cl_2$.

As the tubulin polymerization assay can be sensitive addition of simple cations and non-specific binding/modifications to the tubulin, we also performed the assay in the presence of an excess of bovine serum albumin (BSA). BSA acts as a non-specific protein substrate and which can absorb/bind the RPC in a non-specific manner and thus compete with tubulin for weakly-bound RPC.[76] BSA has shown to bind nonspecifically to tubulin, by displaying multiple binding sites in various crystal structures, docking studies, etc.[71]

As shown in Figure 3.6, the tubulin polymerization curves in the presence of BSA and the RPCs show a less pronounced, but still observable MSA effect. The differences between RPCs are less substantial as they are more clumped together, but a closer examination reveals the same relative order of MSA activity: PTX>> $[Ru(dip)_2phen]Cl_2$ > $[Ru(dip)_3]Cl_2$ > $[Ru(phen)_3]Cl_2$ ~ $[Ru(phen)_2dip]Cl_2$. In fact, in this case, the MSA activity of the last two, $[Ru(phen)_3]Cl_2$ and $[Ru(phen)_2dip]Cl_2$ is barely different than the control, suggesting little specific binding to tubulin.

Along with the ITC calorimetry data that reveals tight specific binding on the order $2X10^5$ M^{-1} (K_a) for $[Ru(dip)_3]Cl_2$ to MTs (Table 3.2), these polymerization curve data show that both specific and non-specific binding are important in the *in vitro* assay, whereas only specific binding is likely to be important *in vivo* or in cellulo. Once non-specific binding is eliminated, only the more hydrophilic RPCs show substantial MSA activity in the *in vitro* assay and these are the most potent cytotoxins. This data in combination with the cellular uptake data, and subcellular localization data, supports a model in which $[Ru(dip)_2phen]Cl_2$ and $[Ru(dip)_3]Cl_2$ are readily transported across the cell membrane and then principally localize with the cytoskeletal proteins due to tight specific binding with tubulin. The other RPCs localize principally in the mitochondria as appears to be common for many RPCs. Thus the presence of at least two dip ligands in the $[Ru(L\text{-}L)_2N\text{-}N]Cl_2$ framework, seems to be the minimum required structure for MSA activity in live cells.

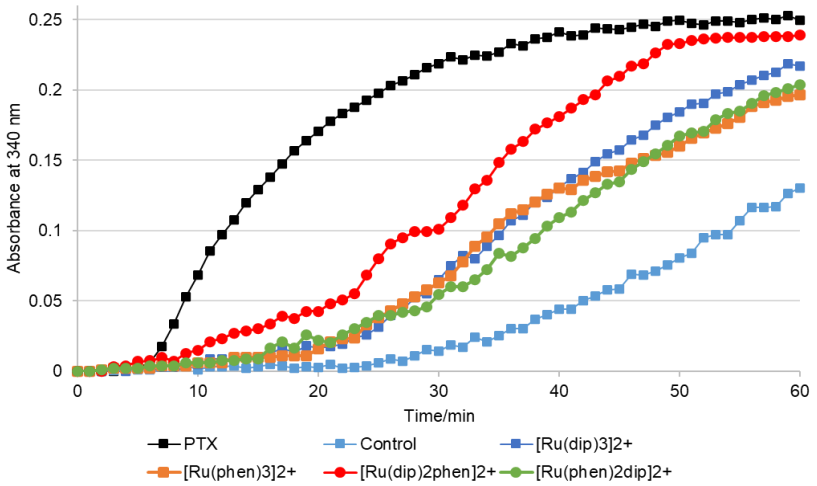

Figure 3.5. The effect of different ligands on tubulin polymerization is done *in vitro* for the family of compounds. The polymerization causes a change in turbidity and is measured by light transmission at 340 nm. The increasing turbidity that indicated by tubulin polymerization occurs upon a temperature jump from 4 ˚C to 37 ˚C in the presence of 1 mM GTP and 10 % glycerol in general tubulin buffer (80 mM PIPES pH 6.9, 2 mM $MgCl_2$, and 0.5 mM EGTA). Runs with an additive (complex) were treated with 10 µM solution and each run contained 3 mg/mL tubulin. The light blue plot shows the normal tubulin polymerization growth curve in the absence of any complex. The black plot represents the microtubule stabilization that occurs in the presence of PTX (MSA). The orange, green, red, and dark blue plot represent the effect on tubulin polymerization in the presence of the family of RPCs $[Ru(phen)_3]Cl_2$, $[Ru(phen)_2dip]Cl_2$, $Ru(dip)_2phen]Cl_2$ and $[Ru(dip)_3]Cl_2$, respectively (color and marker indicated in the legend). The plots in this graph are an average of three experiments; error bars (±0.05 OD) are omitted for clarity.

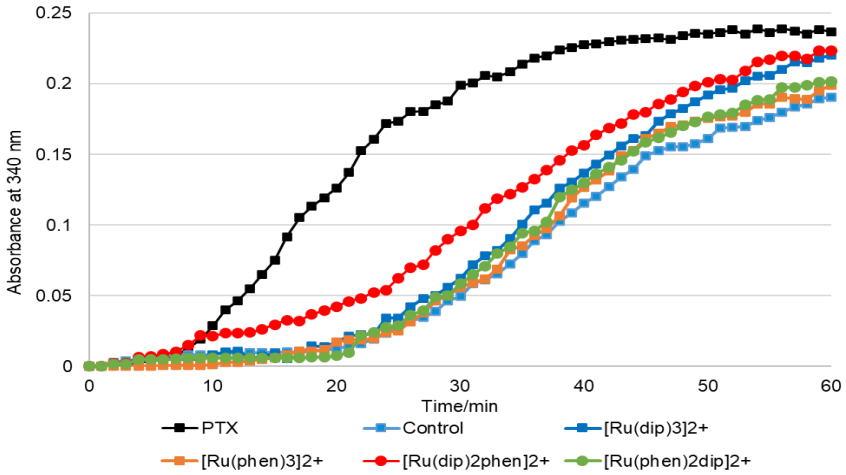

Figure 3.6. The effect of different ligands on tubulin polymerization is done *in vitro* for the family of compounds in the presence of BSA. The polymerization causes a change in turbidity and is measured by light transmission at 340 nm. The increasing turbidity that indicated by tubulin polymerization occurs upon a temperature jump from 4 ˚C to 37 ˚C in the presence of 1 mM GTP and 10 % glycerol in general tubulin buffer (80 mM PIPES pH 6.9, 2 mM $MgCl_2$, and 0.5 mM EGTA). Runs with an additive (complex) were treated with 10 µM solution, 80 µM BSA solution and each run contained 3 mg/mL tubulin. The light blue plot shows the normal tubulin polymerization growth curve only in the presence of BSA. The black plot represents the microtubule stabilization that occurs in the presence of PTX (MSA) with BSA present. The orange, green, red, and dark blue plot represent the effect on tubulin polymerization in the presence of the BSA and the family of RPCs $[Ru(phen)_3]Cl_2$, $[Ru(phen)_2dip]Cl_2$, $Ru(dip)_2phen]Cl_2$ and $[Ru(dip)_3]Cl_2$, respectively (color and marker indicated in the legend). The plots in this graph are an average of three experiments; error bars (±0.05 OD) are omitted for clarity.

From the ITC titration curve, it was also plausible to suggest a binding stoichiometry of 1:1 $[Ru(dip)_3]Cl_2$ to tubulin. Moreover, a competition study in which a pre-formed MT was saturated with DTX and then titrated with $[Ru(dip)_3]Cl_2$ revealed an increase in the K_a for the RPC to $5.0x10^5$ $M^{-}1$, indicating separate binding sites for the two ligands (Table 3.2).[31]

While the titration data can suggest the binding stoichiometry we wanted to develop another method to investigate the suggestive 1:1 $[Ru(dip)_3]^{2+}$:Tubulin stoichiometry.

The binding stoichiometry assay was developed from the tubulin polymerization assay and a modified version of the microtubule-pelleted assay by Murphy et al. while using BSA to aid in non-specific binding.[70] In this experiment, 3 different samples were used (in triplicate): a tubulin control, Ru/BSA, and Tubulin/BSA/Ru. The tubulin control was used to indicate that tubulin polymerization occurred under normal conditions, with no additive. The Ru/BSA was used to ensure no Ru was bound to BSA and pelleted during the experiment. This control was found to have some Ru and BSA in the pellet which was subtracted from the Tubulin/BSA/Ru sample. The concentration for the Ru was simply determined from Beer's Law, and any dilutions were accounted for. Whereas the pellet OD reading from BSA analysis was calculated by using the OD reading and the previously made calibration curve, taking account for dilutions, and converting mg/mL to nmol using the protein's molecular weight.

This experiment was originally performed with $[Ru(dip)_3]Cl_2$. However, due to its high lipophilic properties, even in the presence of BSA the full Ru was not able to be recovered. Therefore, the more water soluble $[Ru(dip)_2phen]Cl_2$ was utilized and

displayed similar MSA as $[Ru(dip)_3]Cl_2$. The data obtained are outlined in Table 3.3, which suggests a 1:1 $[Ru(dip)_2phen]^{2+}$:Tubulin stoichiometry with a protein:Ru 4.6:4.5.

Table 3.2. ITC thermodynamic binding data for $[Ru(dip)_3]^{2+}$, DTX, and colchicine with both tubulin and preformed microtubules done previously in the MacDonnell lab (reported as association constants, Tubulin + Complex $\rightleftharpoons$ Tubulin-Complex).[31]

Complex	Ligand	K_a (M^{-1}) X10^5
Tubulin	DTX	1.2
MT	DTX	1.8
MT	Colchicine	2.0
MT	$[Ru(dip)_3]^{2+}$	2.0
MT:DTX	$[Ru(dip)_3]^{2+}$	5.0

Table 3.3. Data obtained to determine the stoichiometry of $Ru(dip)_2phen]Cl_2$ (indicated as "Ru") to tubulin in the presence of albumin (BSA). Protein in the pellet was determined by BSA and reported as nmol. Ru concentration in the pellet was determined using UV-Vis spectrometer and Beer's Law, which is reported as nmol. "Ru/BSA" was subtracted from "Tubulin/BSA/Ru" and the remainder was reported as "corrected BSA/Ru".

Protein	[Protein]	[Ru]
Tubulin Control	3.0 ± 0.9 nmol	
Ru/BSA	2.0 ± 0.8 nmol	1.0 ± 0.9 nmol
Tubulin/BSA/Ru	6.6 ± 0.5 nmol	5.5 ± 0.6 nmol
Corrected BSA/Ru	4.6 ± 0.5 nmol	4.5 ± 0.6 nmol

3.7 Conclusion

We have performed a mini structure activity relationship of a family of RPCs by altering the ancillary ligands from dip to phen. The difference between the phen and the dip ligands is di-phenyl substituents on the dip ligand. It was found that as the number of dip ligands increased, so did the lipophilicity, cytotoxicity, and uptake. By just changing one of the ligands on the complex $[Ru(phen)_3]Cl_2$ to a dip ligand ($[Ru(phen)_2dip]Cl_2$), the LogP value changed from -1.1 to 1.2 which indicates the strong lipophilic properties this dip ligand creates. Whereas, by just changing one of the ligands on the complex

$[Ru(dip)_3]Cl_2$ to a phen ligand ($[Ru(dip)_2phen]Cl_2$), this complex's solubility is enhanced (now soluble in water) which indicates the hydrophilic properties this phen ligand creates. Throughout this study the dip ligand has seen to play a vital role in biological activity, specifically two dip ligands. By keeping two of the three dip ligands coordinated to Ru in general, cytotoxicity, uptake, sub-cellular localization, and MTA was fairly maintained. This is suggestive that the dip containing ligand has a strong correlation to the cytoskeleton proteins.

This is the first attempt at a SAR study with investigated MT on metallo-based complexes. Even though there is a lot more to be investigated about the MSA of these compounds, these Ru-based that target the cytoskeleton are very promising. Further SAR studies with Ru complexes containing two dip ligands and one hydrophilic ligand as well as Ru complexes with various charges (+1, +3) would be valuable. These types of studies are likely to introduce a new class of metallo-based complexes that target MTs in cells that are synthetically accessible.

APPENDIX

A. NMR data

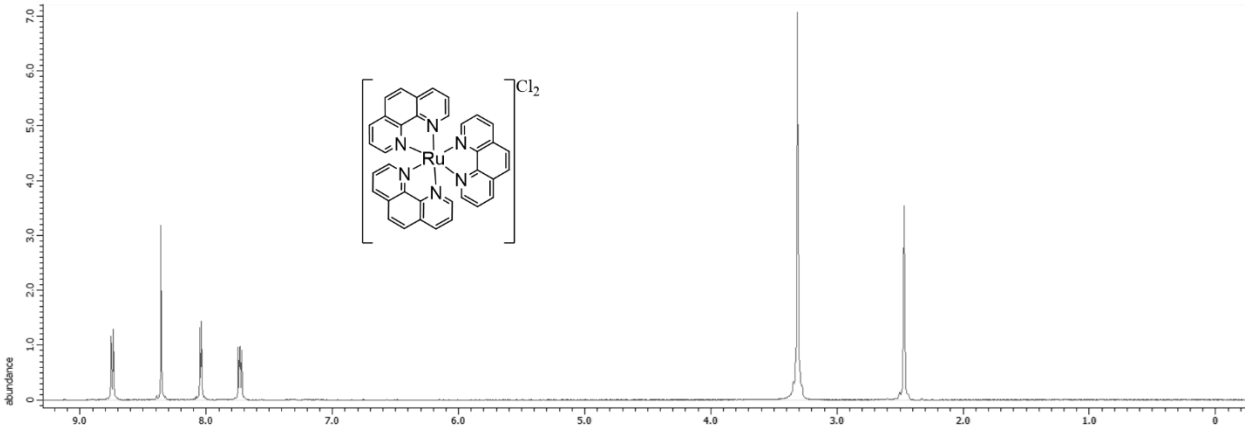

Figure A.1. 1H NMR of $[Ru(phen)_3]Cl_2$ in DMSO.

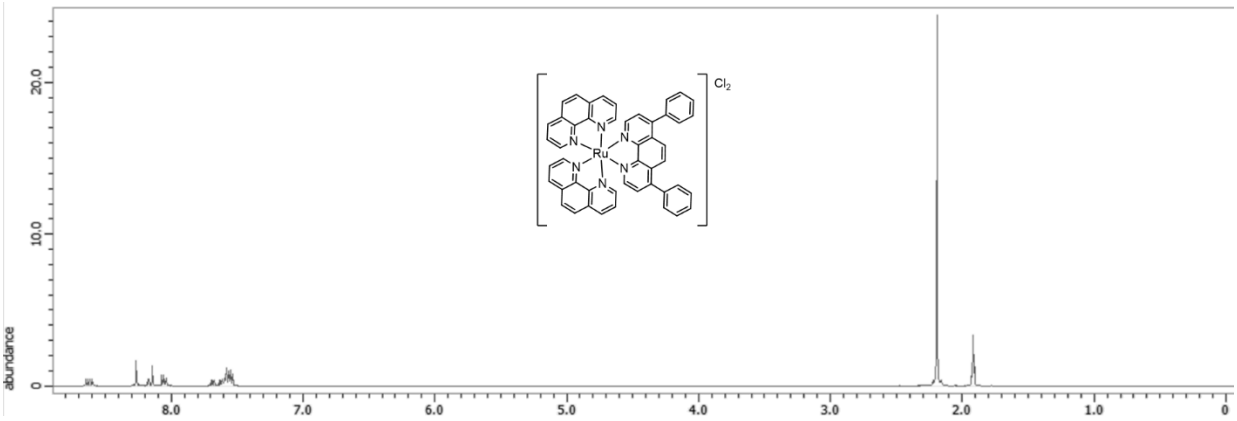

Figure A.2. 1H NMR of $[Ru(phen)_2dip]Cl_2$ in CD_3CN.

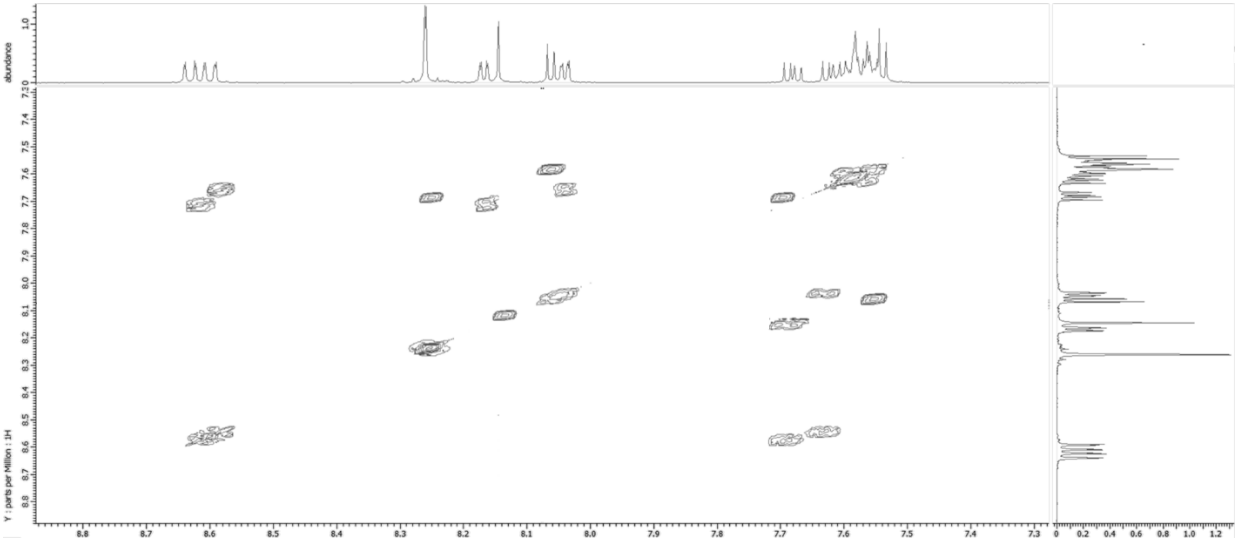

Figure A.3. COSY 1H NMR of $[Ru(phen)_2dip]Cl_2$ in CD_3CN.

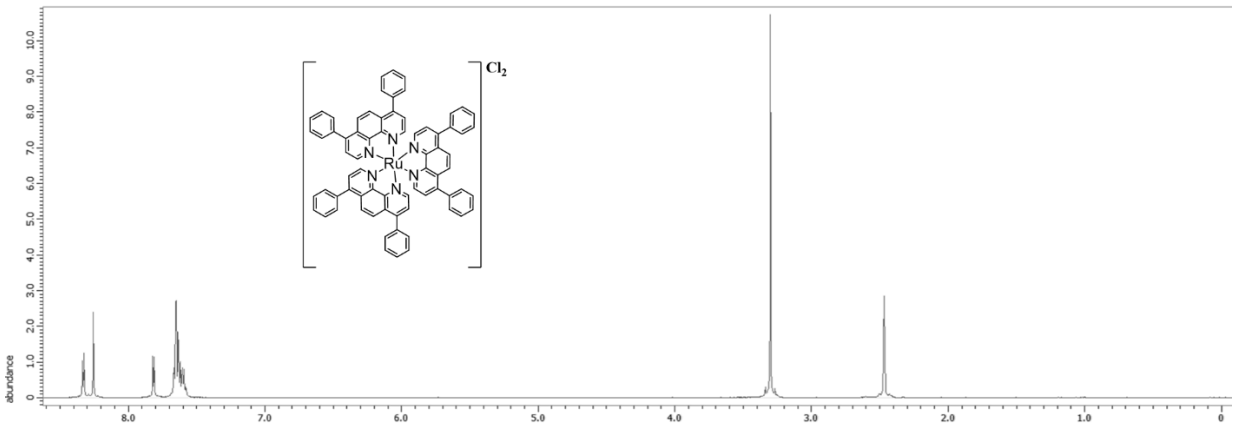

Figure A.4. 1H NMR of $[Ru(dip)_3]Cl_2$ in DMSO.

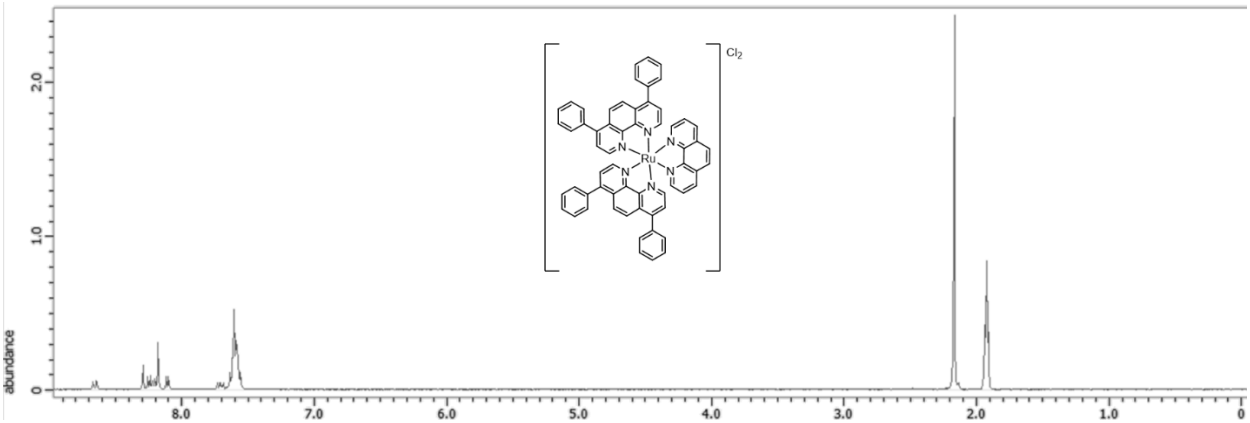

Figure A.5. 1H NMR of $[Ru(dip)_2phen]Cl_2$ in CD_3CN.

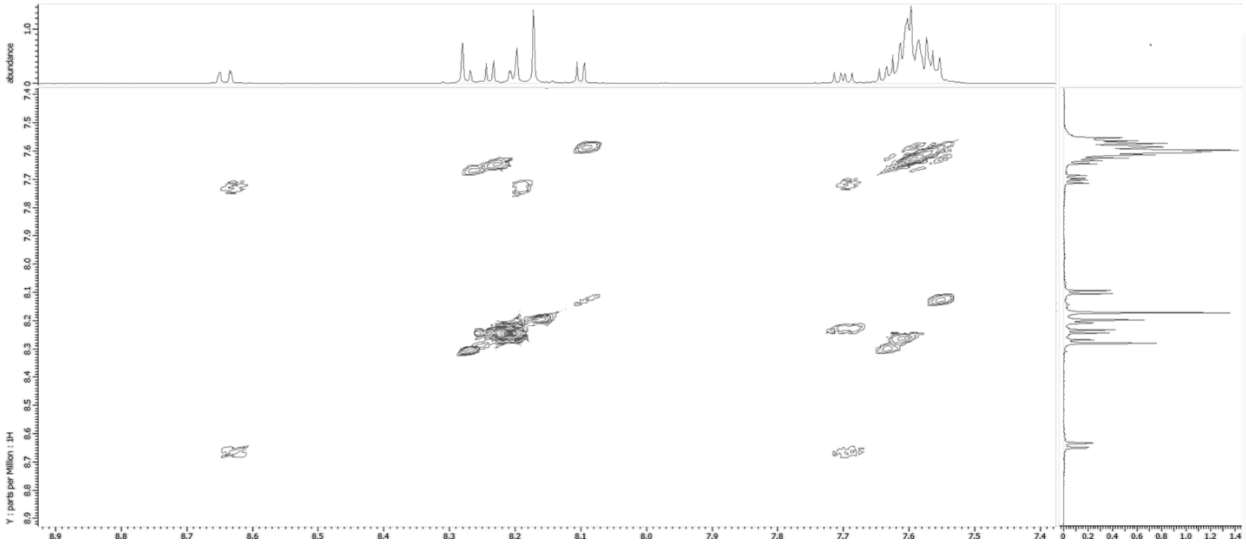

Figure A.6. COSY 1H NMR of $[Ru(dip)_2phen]Cl_2$ in CD_3CN.

B. X-ray crystallography data

Table A.1. Atomic coordinates and equivalent displacement parameters U_{eq} (Å^2) for the $C_{48}H_{40}Cl_2N_6O_4Ru_1$ crystal structure

Atom	x	y	z	U_{eq}
Ru1	0.22491(2)	0	-1/4	0.01635(8)
Cl1	0.16880(6)	-0.87086(5)	-0.48792(4)	0.0305(2)
N1	0.21812(18)	-0.10781(13)	-0.29309(11)	0.0178(6)
N2	0.33857(14)	-0.97701(12)	-0.31019(10)	0.0113(5)
C1	0.2728(2)	-0.14587(14)	-0.34260(14)	0.0204(6)
C2	0.2579(2)	-0.21950(16)	-0.36494(17)	0.0232(8)
C3	0.1888(2)	-0.74382(15)	-0.16366(15)	0.0208(7)
C4	0.1316(2)	-0.78421(16)	-0.21683(17)	0.0222(8)
C5	0.0550(2)	-0.75463(18)	-0.25349(19)	0.0274(9)
C6	0.0018(3)	-0.79160(18)	-0.30299(19)	0.0289(9)
C7	0.02098(19)	-0.86850(19)	-0.32792(16)	0.0240(8)
C8	0.0925(2)	-0.89877(15)	-0.29379(14)	0.0188(7)
N3	0.11675(16)	-0.97073(14)	-0.31297(12)	0.0173(6)
C9	0.0654(2)	-0.01225(19)	-0.36470(14)	0.0221(8)
C10	-0.00661(20)	-0.9838(2)	-0.39856(17)	0.0266(9)
C11	-0.0308(2)	-0.91372(17)	-0.38329(16)	0.0256(8)
C12	0.14996(19)	-0.85828(14)	-0.23816(14)	0.0164(6)
C13	0.42684(17)	-0.98727(15)	-0.28283(12)	0.0149(6)
C14	0.51453(17)	-0.97089(16)	-0.31420(13)	0.0166(7)
C15	0.60124(19)	-0.98408(16)	-0.27955(13)	0.0194(7)
C16	0.50879(18)	-0.93974(14)	-0.37587(12)	0.0143(6)
C17	0.41701(17)	-0.92990(15)	-0.40219(12)	0.0148(6)
C18	0.33520(18)	-0.95040(15)	-0.36934(13)	0.0158(6)
C19	0.59547(17)	-0.91669(16)	-0.41100(14)	0.0179(7)
C20	0.66759(18)	-0.96401(18)	-0.43729(14)	0.0207(7)
C21	0.7471(2)	-0.94095(18)	-0.47283(15)	0.0223(7)
C22	0.7523(2)	-0.87087(18)	-0.48272(17)	0.0233(7)
C23	0.6785(2)	-0.82284(18)	-0.45625(17)	0.0249(8)
C24	0.5988(2)	-0.84660(16)	-0.42197(15)	0.0215(7)
O1	0.3819	-0.8314	-0.5829	0.047723
O2	0.1331	-0.8512	-0.6692	0.098449
O2H1	0.183	-0.8511	-0.6392	0.037995
O2H2	0.0794	-0.8511	-0.642	0.037995
O1H1	0.3814	-0.7814	-0.5829	0.037995
O1H2	0.4219	-0.8494	-0.6189	0.037995
H1C1	0.3231	-0.1229	-0.3635	0.024441
H1C2	0.2979	-0.2453	-0.4018	0.027841
H1C3	0.18	-0.6934	-0.1482	0.024945
H1C5	0.043	-0.7043	-0.2402	0.032887
H1C6	-0.0496	-0.769	-0.3232	0.034718
H1C9	0.0795	-0.0622	-0.3778	0.026474
H1C10	-0.0417	-1.015	-0.4349	0.031942
H1C11	-0.0807	-0.8952	-0.4087	0.030745
H1C15	0.6609	-0.9706	-0.2976	0.023322
H1C17	0.4104	-0.9088	-0.4433	0.017713
H1C18	0.2741	-0.9451	-0.3903	0.019015
H1C20	0.6639	-1.0127	-0.4315	0.024797
H1C21	0.7975	-0.9739	-0.4901	0.026791
H1C22	0.8056	-0.8554	-0.5073	0.027949
H1C23	0.6822	-0.774	-0.4615	0.029843
H1C24	0.547	-0.8145	-0.4062	0.025766

Table A.2. Anisotropic Atomic Displacement Parameters (Å^2) for the $C_{48}H_{40}Cl_2N_6O_4Ru_1$ crystal structure.

Atom	U_{11}	U_{22}	U_{33}	U_{12}	U_{13}	U_{23}
Ru1	0.01835(14)	0.01304(14)	0.01823(12)	0	0	0.00444(9)
Cl1	0.0326(4)	0.0196(3)	0.0392(4)	-0.0034(3)	-0.0028(3)	0.0053(3)
N1	0.0153(9)	0.0141(10)	0.0240(9)	-0.0028(9)	-0.0010(7)	0.0035(8)
N2	0.0079(8)	0.0077(9)	0.0192(8)	0.0035(7)	-0.0023(6)	0.0045(7)
C1	0.0200(11)	0.0094(10)	0.0313(11)	0.0057(11)	0.0030(10)	0.0029(9)
C2	0.0198(13)	0.0122(11)	0.0367(13)	0.0042(10)	-0.0043(9)	0.0028(10)
C3	0.0242(12)	0.0067(10)	0.0299(12)	-0.0027(10)	-0.0011(9)	-0.0002(10)
C4	0.0230(13)	0.0104(12)	0.0343(13)	0.0043(10)	-0.0008(9)	0.0070(11)
C5	0.0247(13)	0.0161(14)	0.0446(15)	0.0045(11)	-0.0019(11)	0.0136(13)
C6	0.0269(15)	0.0192(14)	0.0430(15)	0.0085(12)	-0.0025(12)	0.0117(13)
C7	0.0092(10)	0.0309(16)	0.0350(13)	0.0039(10)	-0.0036(9)	0.0140(12)
C8	0.0198(11)	0.0111(11)	0.0250(11)	0.0037(10)	-0.0063(9)	0.0021(9)
N3	0.0109(9)	0.0160(11)	0.0262(10)	0.0013(8)	-0.0028(7)	0.0071(9)
C9	0.0181(12)	0.0279(15)	0.0216(10)	-0.0018(11)	-0.0069(8)	0.0083(10)
C10	0.0086(11)	0.0365(18)	0.0365(13)	-0.0064(11)	-0.0076(9)	0.0115(13)
C11	0.0344(16)	0.0114(12)	0.0300(13)	-0.0023(12)	-0.0116(11)	0.0015(11)
C12	0.0168(11)	0.0059(10)	0.0274(11)	-0.0002(9)	-0.0016(8)	0.0055(9)
C13	0.0102(10)	0.0191(13)	0.0168(9)	0.0036(8)	-0.0017(7)	0.0068(9)
C14	0.0088(10)	0.0200(13)	0.0230(10)	-0.0032(9)	0.0036(7)	0.0096(10)
C15	0.0163(11)	0.0237(14)	0.0210(10)	-0.0053(10)	0.0029(8)	0.0110(10)
C16	0.0207(11)	0.0080(10)	0.0138(9)	0.0001(9)	0.0009(7)	0.0007(8)
C17	0.0110(9)	0.0151(11)	0.0185(9)	-0.0037(8)	0.0022(7)	0.0041(9)
C18	0.0126(10)	0.0131(11)	0.0232(10)	-0.0004(9)	-0.0020(7)	0.0069(9)
C19	0.0067(9)	0.0207(13)	0.0308(11)	0.0042(9)	0.0029(8)	0.0164(11)
C20	0.0128(10)	0.0233(14)	0.0273(11)	-0.0002(10)	0.0002(8)	0.0084(11)
C21	0.0175(11)	0.0257(14)	0.0259(11)	-0.0004(10)	0.0045(8)	0.0102(11)
C22	0.0178(11)	0.0204(13)	0.0331(13)	-0.0054(10)	-0.0017(8)	0.0085(11)
C23	0.0185(12)	0.0230(15)	0.0365(13)	0.0006(11)	-0.0022(10)	0.0139(12)
C24	0.0210(12)	0.0148(12)	0.0317(12)	-0.0002(10)	0.0045(9)	0.0123(11)

Table A.3. Main Atomic Distance (Å) for the $C_{48}H_{40}Cl_2N_6O_4Ru_1$ crystal structure.

Ru1-N1	2.0674(18)
Ru1-N1(i)	2.0674(18)
Ru1-N2(ii)	2.0655(17)
Ru1-N2(iii)	2.0655(17)
Ru1-N3(ii)	2.084(2)
Ru1-N3(iii)	2.084(2)
N1-C1	1.323(3)
N1-C12(iii)	1.358(3)
N2-C13	1.372(3)
N2-C18	1.332(3)
C1-C2	1.404(4)
C1-H1C1	0.9599
C2-C3(iii)	1.372(4)
C2-H1C2	0.9606
C3-C4	1.404(4)
C3-H1C3	0.9597
C4-C5	1.458(5)
C4-C12	1.419(4)
C5-C6	1.302(5)
C5-H1C5	0.9594
C6-C7	1.479(5)
C6-H1C6	0.9597
C7-C8	1.384(4)
C7-C11	1.430(5)
C8-N3	1.394(3)
C8-C12	1.437(3)

N3-C9(iv)	1.351(3)
C9-C10(ii)	1.370(5)
C9-H1C9	0.959
C10-C11	1.358(5)
C10-H1C10	0.9596
C11-H1C11	0.9593
C13-C13(v)	1.436(3)
C13-C14	1.430(4)
C14-C15	1.431(4)
C14-C16	1.430(4)
C15-C15(v)	1.387(4)
C15-H1C15	0.9611
C16-C17	1.408(4)
C16-C19	1.496(4)
C17-C18	1.401(4)
C17-H1C17	0.9599
C18-H1C18	0.9603
C19-C20	1.384(4)
C19-C24	1.398(6)
C20-C21	1.421(4)
C20-H1C20	0.9603
C21-C22	1.390(6)
C21-H1C21	0.9611
C22-C23	1.410(4)
C22-H1C22	0.9607
C23-C24	1.416(5)
C23-H1C23	0.959
C24-H1C24	0.9597
O1-O1H2	0.9034
O2-O2H1	0.9049
O2-O2H2	0.9159

Table A.4. Main Bonds Angles (˚) for the $C_{48}H_{40}Cl_2N_6O_4Ru_1$ crystal structure.

N1-Ru1-N1(i)	174.71(11)
N1-Ru1-N2(ii)	96.69(9)
N1-Ru1-N2(iii)	87.40(9)
N1-Ru1-N3(ii)	95.42(8)
N1-Ru1-N3(iii)	80.70(8)
N1(i)-Ru1-N2(ii)	87.40(9)
N1(i)-Ru1-N2(iii)	96.69(9)
N1(i)-Ru1-N3(ii)	80.70(8)
N1(i)-Ru1-N3(iii)	95.42(8)
N2(ii)-Ru1-N2(iii)	79.09(7)
N2(ii)-Ru1-N3(ii)	97.19(8)
N2(ii)-Ru1-N3(iii)	175.59(8)
N2(iii)-Ru1-N3(ii)	175.59(8)
N2(iii)-Ru1-N3(iii)	97.19(8)
N3(ii)-Ru1-N3(iii)	86.63(10)
Ru1-N1-C1	128.78(18)
Ru1-N1-C12(iii)	112.35(14)
C1-N1-C12(iii)	118.79(18)
Ru1(iv)-N2-C13	114.67(15)
Ru1(iv)-N2-C18	127.44(15)
C13-N2-C18	117.79(19)
N1-C1-C2	120.7(2)
N1-C1-H1C1	119.58

C2-C1-H1C1	119.7
C1-C2-C3(iii)	122.9(3)
C1-C2-H1C2	118.51
C3(iii)-C2-H1C2	118.56
C2(iii)-C3-C4	116.2(2)
C2(iii)-C3-H1c3	121.85
C4-C3-H1C3	121.92
C3-C4-C5	124.1(3)
C3-C4-C12	118.9(3)
C5-C4-C12	117.0(3)
C4-C5-C6	124.6(4)
C4-C5-H1C5	117.67
C6-C5-H1C5	117.77
C5-C6-C7	119.7(4)
C5-C6-H1C6	120.12
C7-C6-H1C6	120.19
C6-C7-C8	117.4(3)
C6-C7-C11	124.5(3)
C8-C7-C11	118.1(3)
C7-C8-N3	122.2(2)
C7-C8-C12	122.9(2)
N3-C8-C12	114.8(2)
Ru1(iv)-N3-C8	112.77(15)
Ru1(iv)-N3-C9(iv)	128.8(2)
C8-N3-C9(iv)	118.2(3)
N3(ii)-C9-C10(ii)	120.6(3)
N3(ii)-C9-H1C9	119.75
C10(ii)-C9-H1C9	119.64
C9(iv)-C10-C11	123.3(3)
C9(iv)-C10-H1C10	118.35
C11-C10-H1C10	118.37
C7-C11-C10	117.5(3)
C7-C11-H1C11	121.29
C10-C11-H1C11	121.24
N1(iii)-C12-C4	122.4(2)
N1(iii)-C12-C8	119.23(18)
C4-C12-C8	118.4(2)
N2-C13-C13(v)	115.8(2)
N2-C13-C14	123.5(2)
C13(v)-C13-C14	120.6(2)
C13-C14-C15	117.4(2)
C13-C14-C16	117.6(2)
C15-C14-C16	125.0(3)
C14-C15-C15(v)	121.7(3)
C14-C15-H1C15	119.08
C15(v)-C15-H1C15	119.2
C14-C16-C17	117.1(2)
C14-C16-C19	122.4(2)
C17-C16-C19	120.6(2)
C16-C17-C18	121.1(2)
C16-C17-H1C17	119.4
C18-C17-H1C17	119.48
N2-C18-C17	122.8(2)
N2-C18-H1C18	118.65
C17-C18-H1C18	118.52
C16-C19-C20	121.9(3)

C16-C19-C24	118.0(3)
C20-C19-C24	119.9(3)
C19-C20-C21	120.3(3)
C19-C20-H1C20	119.79
C21-C20-H1C20	119.87
C20-C21-C22	120.3(3)
C20-C21-H1C21	119.82
C22-C21-H1C21	119.85
C21-C22-C23	119.3(3)
C21-C22-H1C22	120.42
C23-C22-H1C22	120.25
C22-C23-C24	119.9(4)
C22-C23-H1C23	120.12
C24-C23-H1C23	119.95
C19-C24-C23	120.1(3)
C19-C24-H1C24	119.96
C23-C24-H1C24	119.94
O2H1-O2-O2H2	105.82

Symmetry elements applied on the independent atomic positions for atomic distances and bond angles:

(i) x,-y,-z-1/2
(ii) x,y+1,z
(iii) x,-y-1,-z-1/2
(iv) x,y-1,z
(v) x,-y-2,-z-1/2

REFERENCES

(1) Cancer Facts & Figures https://www.cancer.org/research/cancer-facts-statistics/all-cancer-facts-figures/cancer-facts-figures-2019.html (accessed Mar 9, 2020).

(2) Ke, X.; Shen, L. Frontiers in Laboratory Medicine Molecular Targeted Therapy of Cancer : The Progress and Future Prospect. *Front. Lab. Med.* **2017**, *1* (2), 69–75. https://doi.org/10.1016/j.flm.2017.06.001.

(3) Tian, B. F.; Turner, E. Drug Resistance in Cancer: Mechanisms and Models. *ATCC White paper*. 2019, pp 8–9.

(4) Allardyce, C. S.; Dyson, P. J. Ruthenium in Medicine : Current Clinical Uses and Future Prospects. *Platin. Met. Rev.* **2001**, *45* (2), 62–69.

(5) Yellepeddi, V. K.; Vangara, K. K.; Kumar, A.; Palakurthi, S. Comparative Evaluation of Small-Molecule Chemosensitizers in Reversal of Cisplatin Resistance in Ovarian Cancer Cells. *Anticaner Res.* **2012**, *32*, 3651–3658.

(6) Astolfi, L.; Ghiselli, S.; Guaran, V.; Chicca, M.; Simoni, E. D. I.; Olivetto, E.; Lelli, G.; Martini, A. Correlation of Adverse Effects of Cisplatin Administration in Patients Affected by Solid Tumours: A Retrospective Evaluation. *Oncol. Rep.* **2013**, *29*, 1285–1292. https://doi.org/10.3892/or.2013.2279.

(7) Alderden, R. A.; Hall, M. D.; Hambley, T. W. Products of Chemistry The Discovery and Development of Cisplatin. *J. Chem. Edu.* **2006**, *83* (5), 728–734. https://doi.org/10.1021/ed083p728.

(8) Hall, M. D.; Telma, K. A.; Chang, K.; Lee, T. D.; Madigan, J. P.; Lloyd, J. R.; Goldlust, I. S.; Hoeschele, J. D.; Gottesman, M. M. Say No to DMSO:

Dimethylsulfoxide Inactivates Cisplatin, Carboplatin, and Other Platinum Complexes. *Cancer Res.* **2014**, *74* (14), 3913–3923. https://doi.org/10.1158/0008-5472.CAN-14-0247.

(9) Shen, D.; Pouliot, L. M.; Hall, M. D.; Gottesman, M. M. Cisplatin Resistance: A Cellular Self-Defense Mechanism Resulting from Multiple Epigenetic and Genetic Changes. *Pharmacol. Rev.* **2012**, *64* (3), 706–721. https://doi.org/10.1124/pr.111.005637.

(10) Galluzzi, L.; Vitale, I.; Michels, J.; Brenner, C.; Szabadkai, G.; Castedo, M. Systems Biology of Cisplatin Resistance: Past, Present and Future. *Cell Death Dis.* **2014**, *5*, 1–18. https://doi.org/10.1038/cddis.2013.428.

(11) Cruz-bermúdez, A.; Laza-briviesca, R.; Vicente-blanco, R. J.; García-grande, A.; José, M.; Laine-menéndez, S.; Palacios-zambrano, S.; Moreno-villa, M. R.; Ruiz-valdepeñas, A. M.; Lendinez, C.; Romero, A.; Franco, F.; Calvo, V.; Alfaro, C.; Martin, P.; Salas, C.; Miguel, J.; Provencio, M. Free Radical Biology and Medicine Cisplatin Resistance Involves a Metabolic Reprogramming through ROS and PGC-1 α in NSCLC Which Can Be Overcome by OXPHOS Inhibition. *Free Radic. Biol. Med.* **2019**, *135*, 167–181. https://doi.org/10.1016/j.freeradbiomed.2019.03.009.

(12) Stordal, B.; Davey, M. Critical Review Understanding Cisplatin Resistance Using Cellular Models. *Life* **2007**, *59* (11), 696–699. https://doi.org/10.1080/15216540701636287.

(13) Florea, A. and Busselberg, D. Cisplatin as an Anti-Tumor Drug: Cellular Mechanisms of Activity, Drug Resistance and Induced Side Effects. *Cancers*

(Basel). **2011**, *3*, 1351–1371. https://doi.org/10.3390/cancers3011351.

(14) Galluzzi, L.; Senovilla, L.; Vitale, I.; Michels, J.; Martins, I.; Kepp, O.; Castedo, M.; Kroemer, G. Molecular Mechanisms of Cisplatin Resistance. *Oncogene* **2012**, *31* (15), 1869–1883. https://doi.org/10.1038/onc.2011.384.

(15) Chen, S. H.; Chang, J. Y. New Insights into Mechanisms of Cisplatin Resistance: From Tumor Cell to Microenvironment. *Int. J. Mol. Sci.* **2019**, *20* (17), 4136–4157. https://doi.org/10.3390/ijms20174136.

(16) Blagosklonny, M. V. Analysis of FDA Approved Anticancer Drugs Reveals the Future of Cancer Therapy. *Cell Cycle Rev.* **2004**, *3* (8), 1035–1042.

(17) Alessio, E. Thirty Years of the Drug Candidate NAMI-A and the Myths in the Field of Ruthenium Anticancer Compounds: A Personal. *Eur. J. Inorg. Chem.* **2017**, 1549–1560. https://doi.org/10.1002/ejic.201600986.

(18) Coverdale, J. P. C.; Laroiya-mccarron, T.; Romero-canel, I. Designing Ruthenium Anticancer Drugs: What Have We Learnt from the Key Drug Candidates? *Inorganics* **2019**, *31* (7), 1–15. https://doi.org/10.3390/inorganics7030031.

(19) Page, S. Ruthenium Compounds as Anticancer Agents. *RSC*. 2012, pp 26–29.

(20) Haas, K. L.; Franz, K. J. Application of Metal Coordination Chemistry To Explore and Manipulate Cell Biology. *Chem. Rev.* **2009**, *109*, 4921–4960. https://doi.org/10.1021/cr900134a.

(21) Zeng, L.; Gupta, P.; Chen, Y.; Wang, E.; Ji, L.; Chao, H. The Development of Anticancer Ruthenium(II) Complexes: From Single Molecule Compounds to Nanomaterials. *Chem Soc Rev.* **2018**, *46* (19), 5771–5804. https://doi.org/10.1039/c7cs00195a.

(22) Narvekar, M.; Xue, H. Y.; Eoh, J. Y.; Wong, H. L. Nanocarrier for Poorly Water-Soluble Anticancer Drugs — Barriers of Translation and Solutions. *AAPS PharmSciTech* **2014**, *15* (4), 822–833. https://doi.org/10.1208/s12249-014-0107-x.

(23) Tan, T. N.; Weston, R. H.; Hogan, J. P. Use of 103Ru-Labelled Tris (1,10-Phenanthroline) Ruthenium (II) Chloride as a Marker in Digestion Studies with Sheep. *Int J Appl Radiat Isot .* **1971**, *22* (5), 301–308. https://doi.org/10.1016/0020-708x(71)90004-4.

(24) Alatrash, N.; Narh, E. S.; Yadav, A.; Kim, M.; Janaratne, T.; Gabriel, J.; Macdonnell, F. M. Synthesis, DNA Cleavage Activity, Cytotoxicity, Acetylcholinesterase Inhibition, and Acute Murine Toxicity of Redox-Active Ruthenium (II) Polypyridyl Complexes. *ChemMedChem* **2017**, *12*, 1–16. https://doi.org/10.1002/cmdc.201700240.

(25) Dwyer, F.; Gyarfas, E.; Rogers, W.; Koch, J. Biological Activity of Complex Ions. *Nature* **1952**, *170*, 190–191.

(26) Puckett, C. A.; Barton, J. K. Methods to Explore Cellular Uptake of Ruthenium Complexes. *JACS* **2007**, *129*, 46–47. https://doi.org/10.1021/ja0677564.

(27) Fujita, T.; Iwasa, J.; Hansch, C. A New Substituent Constant, Pi, Derived from Partition Coefficients. *JACS* **1964**, *86* (23). https://doi.org/10.1021/ja01077a028.

(28) Dickerson, M.; Sun, Y.; Howerton, B.; Glazer, E. C. Modifying Charge and Hydrophilicity of Simple Ru(II) Polypyridyl Complexes Radically Alters Biological Activities: Old Complexes, Surprising New Tricks. *Inorg. Chem.* **2014**, *53*, 10370–10377. https://doi.org/10.1021/ic5013796.

(29) Alatrash, N. PhD: Redox Active Lipophilic Ruthenium Complexes as Potenital Anticancer Drugs, University of Texas at Arlginton, 2015.

(30) Gill, M. R.; Derrat, H.; Smythe, C. G. W.; Battaglia, G.; Thomas, J. A. Ruthenium(II) Metallo-Intercalators: DNA Imaging and Cytotoxicity. *ChemBioChem* **2011**, *12* (6), 877–880. https://doi.org/10.1002/cbic.201000782.

(31) Alatrash, N.; Issa, F. H.; Bawazir, N. S.; West, S. J.; Van Manen-Brush, K. E.; Shelor, C. P.; Dayoub, A. S.; Myers, K. A.; Janetopoulos, C.; Lewis, E. A.; MacDonnell, F. M. Disruption of Microtubule Function in Cultured Human Cells by a Cytotoxic Ruthenium(II) Polypyridyl Complex. *Chem. Sci.* **2020**, *11* (1), 264–275. https://doi.org/10.1039/c9sc05671h.

(32) Guo, X.; Zhang, X.; Li, Y.; Guo, Y.; Wang, J.; Li, Y.; Shen, B.; Sun, D.; Zhang, J. Nocodazole Increases the ERK Activity to Enhance MKP-1 Expression Which Inhibits P38 Activation Induced by TNF-α. *Mol. Cell. Biochem.* **2012**, *364*, 373–380. https://doi.org/10.1007/s11010-012-1239-5.

(33) Vantard, M.; Lambert, A. M.; Mey, J. De; Picquot, P.; Van Eldik, L. J. Characterization and Immunocytochemical Distribution of Calmodulin in Higher Plant Endosperm Cells: Localization in the Mitotic Apparatus. *J. Cell Biol.* **1985**, *101*, 488–499. https://doi.org/10.1083/jcb.101.2.488.

(34) Mcnamara, D. E.; Senese, S.; Yeates, T. O.; Torres, J. Z. Structures of Potent Anticancer Compounds Bound to Tubulin. *Protein Soc.* **2015**, *24*, 1164–1172. https://doi.org/10.1002/pro.2704.

(35) Manfredi, J. J.; Parness, J.; Horwitz, S. B. Taxol Binds to Cellular Microtubules. *J. Cell Biol.* **1982**, *94*, 688–696. https://doi.org/10.1083/jcb.94.3.688.

(36) Shelanski, M. L.; Gaskint, F.; Cantort, C. R. Microtubule Assembly in the Absence of Added Nucleotides. *Proc. Nat. Acad. Sci. USA* **1973**, *70* (3), 765–768. https://doi.org/10.1073/pnas.70.3.765.

(37) Karahalil, B.; Yardım-akaydin, S.; Baytas, S. N. An Overview of Microtubule Targeting Agents for Cancer Therapy. *Arh Hig Rada Toksikol* **2019**, *70* (5), 160–172. https://doi.org/10.2478/aiht-2019-70-3258.

(38) The Cytoskeleton https://www.khanacademy.org/science/biology/structure-of-a-cell/tour-of-organelles/a/the-cytoskeleton. (accessed Mar 17, 2020).

(39) Celebier, M.; Kocak, E.; Dogan, A.; Altınoz, S.; Bascı, N. Investigating the Physicochemical Properties of Phenazopyridine Hydrochloride Using High-Performance Liquid Chromatography and UV-Visible Spectrophotometry. *Marmara Pharm J.* **2018**, *22* (4), 528–535. https://doi.org/10.12991/jrp.2018.94.

(40) Gill, M. R.; Jarman, P. J.; Halder, S.; Walker, M. G.; Saeed, H. K.; Thomas, J. A.; Smythe, C.; Ramadan, K.; Vallis, K. A. A Three-in-One-Bullet for Oesophageal Cancer: Replication Fork Collapse, Spindle Attachment Failure and Enhanced Radiosensitivity Generated by a Ruthenium(II) Metallo-Intercalator. *Chem. Sci.* **2018**, *9* (4), 841–849. https://doi.org/10.1039/c7sc03712k.

(41) Thier, R.; Bonacker, D.; Stoiber, T.; Böhm, K. J.; Wang, M.; Unger, E.; Bolt, H. M.; Degen, G. Interaction of Metal Salts with Cytoskeletal Motor Protein Systems. *Toxicol. Lett.* **2003**, *140–141*, 75–81. https://doi.org/10.1016/S0378-4274(02)00502-7.

(42) Stoiber, T.; Bonacker, D.; Böhm, K. J.; Bolt, H. M.; Thier, R.; Degen, G. H.; Unger, E. Disturbed Microtubule Function and Induction of Micronuclei by Chelate

Complexes of Mercury(II). *Mutat. Res. - Genet. Toxicol. Environ. Mutagen.* **2004**, *563* (2), 97–106. https://doi.org/10.1016/j.mrgentox.2004.06.009.

(43) Li, Y. M.; Broome, J. D. Arsenic Targets Tubulins to Induce Apoptosis in Myeloid Leukemia Cells. *Cancer Res.* **1999**, *59* (4), 776–780.

(44) Olmsted, J. B.; Borisy, G. G. Ionic and Nucleotide Requirements for Microtubule Polymerization in Vitro. *Biochemistry* **1975**, *14* (13), 2996–3005. https://doi.org/10.1021/bi00684a032.

(45) Qin, T.; Li, J.; Yuan, M.; Mao, T. Characterization of the Role of Calcium in Regulating the Microtubule-Destabilizing Activity of MDP25. *Plant Signal. Behav.* **2012**, *7* (7), 708–710. https://doi.org/10.4161/psb.20336.

(46) Hepler, P. K. The Cytoskeleton and Its Regulation by Calcium and Protons. *Plant Physiol.* **2016**, *170* (1), 3–22. https://doi.org/10.1104/pp.15.01506.

(47) Deinum, J.; Wallin, M.; Jensen, P. W. The Binding of Ruthenium Red to Tubulin. *BBA - Gen. Subj.* **1985**, *838* (2), 197–205. https://doi.org/10.1016/0304-4165(85)90079-0.

(48) Deinum, J.; Wallin, M.; Kanje, M.; Lagercrantz, C. The Effect of Ruthenium Red on the Assembly and Disassembly of Microtubles and on Rapid Axonal Transport. *BBA - Gen. Subj.* **1981**, *675* (2), 209–213. https://doi.org/10.1016/0304-4165(81)90228-2.

(49) Kong, K. V.; Liao, L. De; Lam, Z.; Thakor, N. V.; Leong, W. K.; Olivo, M. Organometallic Carbonyl Clusters: A New Class of Contrast Agents for Photoacoustic Cerebral Vascular Imaging. *Chem. Commun.* **2014**, *50* (20), 2601–2603. https://doi.org/10.1039/c3cc48529c.

(50) Alatrash, N. MS: Increasing Lipophilicity of Redox Active Ruthenium Complexes as a Means to Enhance Cytotoxicity and Reduce Animal Toxicity, University of Texas at Arlington, 2012.

(51) Puckett, C. A.; Barton, J. K. Mechanism of Cellular Uptake of a Ruthenium Polypyridyl Complex. *Biochemistry* **2008**, *47*, 11711–11716. https://doi.org/10.1021/bi800856t.

(52) Sullivan, B. P.; Salmon, D. J.; Meyer, T. J. Mixed Phosphine 2,2'-Bipyridine Complexes of Ruthenium. *Inorg. Chem.* **1978**, *17* (12), 3334–3341. https://doi.org/10.1021/ic50190a006.

(53) Barton, J. K. United States Patent (19). 5,157,032, 1992.

(54) Bosnich, B. and Dwyer, F. P. Bis-1,10-Phenanthroline Complexes of Divalent Ruthenium. *Aust. J. Chem.* **1966**, *19* (12), 2229–2233. https://doi.org/https://doi.org/10.1071/CH9662229.

(55) Reardon, M. M.; MacDonnell, F. Experimental Crystal Structure Determination (2049829). *CCDC*. https://doi.org/DOI: 10.5517/ccdc.csd.cc26t0jl.

(56) Hansch, C.; Anderson, S. M. The Effect of Intramolecular Hydrophobic Bonding on Partition Coefficients. *J. Org. Chem.* **1967**, *32* (8), 2583–2586. https://doi.org/10.1021/jo01283a049.

(57) Camenisch, G.; Alsenz, J.; Van De Waterbeemd, H.; Folkers, G. Estimation of Permeability by Passive Diffusion through Caco-2 Cell Monolayers Using the Drugs' Lipophilicity and Molecular Weight. *Eur. J. Pharm. Sci.* **1998**, *6* (4), 313–319. https://doi.org/10.1016/S0928-0987(97)10019-7.

(58) Puckett, C. A. The Cellular Uptake of Luminescent Ruthenium Complexes,

California Institute of Technology, 2010.

(59) Pisani, M. J.; Fromm, P. D.; Mulyana, Y.; Clarke, R. J.; Körner, H.; Heimann, K.; Collins, J. G.; Keene, F. R. Mechanism of Cytotoxicity and Cellular Uptake of Lipophilic Inert Dinuclear Polypyridyl Ruthenium(II) Complexes. *ChemMedChem* **2011**, *6* (5), 848–858. https://doi.org/10.1002/cmdc.201100053.

(60) Jarman, P. J.; Noakes, F.; Fairbanks, S.; Smitten, K.; Gri, I. K.; Saeed, H. K.; Thomas, J. A.; Smythe, C. Exploring the Cytotoxicity, Uptake, Cellular Response, and Proteomics of Mono- and Dinuclear DNA Light-Switch Complexes. *JACS* **2019**. https://doi.org/10.1021/jacs.8b09999.

(61) Lai, S.; Jiang, G.; Yao, J.; Li, W.; Han, B.; Zhang, C. Cytotoxic Activity , DNA Damage , Cellular Uptake , Apoptosis and Western Blot Analysis of Ruthenium (II) Polypyridyl Complex against Human Lung Decarcinoma A549 Cell. *J. Inorg. Biochem.* **2015**, *152*, 1–9. https://doi.org/10.1016/j.jinorgbio.2015.08.012.

(62) Zava, O.; Zakeeruddin, S. M.; Danelon, C.; Vogel, H.; Grätzel, M.; Dyson, P. J. A Cytotoxic Ruthenium Tris(Bipyridyl) Complex That Accumulates at Plasma Membranes. *ChemBioChem* **2009**, *10* (11), 1796–1800. https://doi.org/10.1002/cbic.200900013.

(63) Pasquier, E.; Kavallaris, M. Critical Review Microtubules: A Dynamic Target in Cancer Therapy. *Life* **2008**, *60* (3), 165–170. https://doi.org/10.1002/iub.25.

(64) Jordan, A.; Hadfield, J. A.; Lawrence, N. J.; Mcgown, A. T. Anticancer Drugs: Agents Which Interact with the Mitotic Spindle. *Med. Res. Rev.* **1998**, *18* (4), 259–296.

(65) Stanton, R. A.; Gernert, K. M.; Nettles, J. H.; Aneja, R. Drugs That Target

Dynamic Microtubules: A New Molecular Perspective. *Med. Res. Rev.* **2011**, *31* (3), 443–481. https://doi.org/10.1002/med.

(66) Einstein, A. ® : The First Microtubule Stabilizing Agent Taxol. *Int. J. Mol. Sci.* **2017**, *18*, 2–11. https://doi.org/10.3390/ijms18081733.

(67) Brabander, A. M. De; Geuens, G.; Nuydens, R.; Willebrords, R.; Mey, J. De; Biological, P.; Sep, S.; Brabander, M. D. E.; Geuens, G.; Nuydens, R.; Will, R. Taxol Induces the Assembly of Free Microtubules in Living Cells and Blocks the Organizing Capacity of the Centrosomes and Kinetochores Published by : National Academy of Sciences Stable URL : Https://Www.Jstor.Org/Stable/11514 Taxol Induces the Assembly O. *PNAS* **2020**, *78* (9), 5608–5612.

(68) Dayoub, A. PhD. Dissertation, Intracellular Biochemical Targets of Ruthenium Polypyridyl Complexes in Multiple Cancer Cell Models, University of Texas at Arlingtion, 2016.

(69) Pierce™ BCA Protein Assay Kit (23225) https://www.thermofisher.com/order/catalog/product/23225#/23225.

(70) Murphy, S. M.; Preble, A. M.; Patel, U. K.; O'Connell, K. L.; Prabha Dias, D.; Moritz, M.; Agard, D.; Stults, J. T.; Stearns, T. GCP5 and GCP6: Two New Members of the Human γ-Tubulin Complex. *Mol. Biol. Cell* **2001**, *12* (11), 3340–3352. https://doi.org/10.1091/mbc.12.11.3340.

(71) Thakur, A.; Patwa, J.; Pant, S.; Sharma, A.; Flora, S. J. S. Interaction Study of Monoisoamyl Dimercaptosuccinic Acid with Bovine Serum Albumin Using Biophysical and Molecular Docking Approaches. *Sci. Rep.* **2021**, *11* (1), 1–14. https://doi.org/10.1038/s41598-021-83534-0.

(72) Thomas, G. W.; Rael, L. T.; Hausburg, M.; Frederick, E. D.; Brody, E.; Bar-Or, D. The Low Molecular Weight Fraction of Commercial Human Serum Albumin Induces Acetylation of α-Tubulin and Reduces Transcytosis in Retinal Endothelial Cells. *Biochem. Biophys. Res. Commun.* **2016**, *478* (4), 1780–1785. https://doi.org/10.1016/j.bbrc.2016.09.026.

(73) Mazuryk, O.; Magiera, K. Multifaceted Interplay between Lipophilicity , Protein Interaction and Luminescence Parameters of Non-Intercalative Ruthenium (II) Polypyridyl Complexes Controlling Cellular Imaging and Cytotoxic Properties. *J Biol Inorg Chem* **2014**, *19*, 1305–1316. https://doi.org/10.1007/s00775-014-1187-5.

(74) QIAGEN. Qproteome Cell Compartment Kit Print https://www.qiagen.com/be/products/discovery-and-translational-research/protein-purification/fractionation-and-depletion/qproteome-cell-compartment-kit/#resources (accessed Feb 6, 2020).

(75) Field, J. J.; Díaz, J. F.; Miller, J. H. The Binding Sites of Microtubule-Stabilizing Agents. *Chem. Biol.* **2013**, *20* (3), 301–315. https://doi.org/10.1016/j.chembiol.2013.01.014.

(76) Taraboletti, G.; Micheletti, G.; Dossi, R.; Borsotti, P.; Martinelli, M.; Fiordaliso, F.; Ryan, A. J.; Giavazzi, R. Potential Antagonism of Tubulin-Binding Anticancer Agents in Combination Therapies. *Clin. Cancer Res.* **2005**, *11* (7), 2720–2726. https://doi.org/10.1158/1078-0432.CCR-04-1616.

(77) Arnst, K. E.; Wang, Y.; Hwang, D.; Xue, Y.; Costello, T.; Hamilton, D.; Chen, Q.; Yang, J.; Park, F.; Dalton, J. T.; Miller, D. D.; Li, W. A Potent , Metabolically

Stable Tubulin Inhibitor Targets the Colchicine Binding Site and Overcomes Taxane Resistance. *Am. Assoc. Cancer Res.* **2018**, *78* (1), 265–278. https://doi.org/10.1158/0008-5472.CAN-17-0577.

(78) Hiort, C.; Norden, B.; Rodger, A. Enantiopreferential DNA Binding of Circular Dichroism. *JACS* **1990**, *112*, 1971–1982. https://doi.org/10.1021/ja00161a050.

BIOLOGICAL INFORMATION

Melissa was born and raised in Fort Lauderdale, Florida. She went to undergraduate in Fort Myers, Florida where she attended Florida Gulf Coast University (FGCU). In Summer 2016, Melissa began her undergraduate research with Dr. Mirjafari, in which she had been an active member of his scholarship initiatives in terms of designing new experiments, characterizing the structural and physicochemical properties of synthesized products, and mentoring students in lab. She synthesized ILs utilizing a novel approach, click-chemistry. In addition, she has also successfully published three papers involving research in: low toxicity in gene delivery, NTf_2 stability in an enzyme, and surface coating agents using ionic liquids. In December 2017, Melissa graduated from FGCU, with a B.S. in Biology and a minor in Chemistry. After Graduating FGCU in Fall 2017, Melissa was offered an internship for the Spring 2018 semester at Algenol in the Chemistry/Engineering/Aquaculture Department, where she aided this biotechnology company as a Chemistry consultant. This company functions by using science and technology to make commercial products from algae, which meets a variety of society's needs. In summer 2018, Melissa worked as a researcher in Dr. MacDonnell's lab at The University of Texas Arlington under the Richard B. Timmons Scholarship, where she later started the graduate program in Fall 2018. She synthesized, purified, and characterized organic and metal-organic complexes, screened metal-complexes against malignant and non-malignant cells lines, investigate complexes' uptake and accumulation, and determine complexes interaction, effect, and stoichiometry with tubulin *in vitro*.

Melissa graduated from The University of Texas at Arlington with her Master's in Chemistry in 2021.